NASA TECHNICAL MEMORANDUM

NASA TM-75243

EXPERIMENTAL STUDY OF THE LAMINAR-TURBULENT TRANSITION OF A CONCAVE WALL IN A PARALLEL FLOW

H. Bippes

(NASA-TM-75243) EXPERIMENTAL STUDY OF THE LAMINAR-TURBULENT TRANSITION OF A CONCAVE WALL IN A PARALLEL FLOW (National Aeronautics and Space Administration) 73 p HC A04/MF A01 CSCL 20D G3/34

N78-21412

Unclas 15898

Translation of "Experimentelle Untersuchung des laminar-turbulenten Umschlags an einer parallel angeströmten konkaven Wand," Heidelberger Akademie der Wissenschaften, Matematisch-naturwissenschaftliche klasse, Sitzungsberichte, no. 3, 1972, pp. 103-180.

NATIONAL AERONAUTICS AND SPACE ADMINISTRATION
WASHINGTON, D.C. 20546 MARCH 1978

Table of Contents

	Page
Notation	iv
Summary	1
1. Introduction	1
2. The Stability of the Boundary Layer Along a Concave Wall	2
2.1 Results of Theoretical Studies	2
2.2 Results of previous Experimental Studies	4
2.3 Aims of these Experiments and their Relationship to Previous Studies	6
3. Test Setup	7
3.1 Water Towing Tank	7
3.2 Models	10
4. Measurement Technique	12
4.1 Hydrogen Bubble Measurement	12
4.1.1 Streaklines and Timelines	13
4.1.2 Power Supply for Producing the Hydrogen Bubbles	14
4.1.3 Illumination	16
4.1.4 Photography	17
4.2 Velocity Measurement Using Photogrammetric Analysis of Hydrogen Bubble Photographs	17
4.2.1 Photogrammetry in a Two-Medium System	19
4.2.2 Photogrammetric Stereocamera Design	21
4.2.3 Picture Coordinate Measurement	23
4.2.4 Accuracy of Measurement	24
4.3 Disturbance Generators	28
4.3.1 Using Screens to Generate Disturbances	29
4.3.2 Using Hot Wires to Generate Disturbances	30
5. Experimental Results	32
5.1 The Instability Occurring in the Boundary Layer on a Concave Wall	32
5.1.1 Experiments without a Disturbance Generator	33
5.1.2 Experiments with Screens	34
5.1.3 Experiments with Heated Wires	36
5.2 Effect of the Wall Curvature	38
5.3 The Wavelength of the Longitudinal Vortex Disturbances	40
5.4 The Neutral Curve	42
5.5 Excitation of the Longitudinal Vortex Disturbance	46
5.5.1 The Relationship between Excitation and Wavelength	47

5.5.2 Quantitative Determination of the Excitation of the Longitudinal Vortex Disturbance 48
5.5.2.1 Velocity Profiles in the Boundary Layer Disturbed by Excited Longitudinal Vortices 48
5.5.2.2 The Excitation Curve 50
5.6 The Laminar-Turbulent Transition 51
5.6.1 The Longitudinal Vortex Field 51
5.6.2 Secondary Instability 53
5.6.3 Sinuous Motion of the Longitudinal Vortex Streets 59

6. Summary 63

7. References 65

Notation /105

x	arc length along the wall, measured from the leading edge
y	distance from the wall
z	span direction, perpendicular to the x-y plane
U_∞	velocity of oncoming flow
U_0	velocity component of the boundary layer main flow
P_0	pressure in the main flow
U,V,W	components of the boundary layer velocity
P	pressure in the boundary layer
u,v,w	longitudinal vortex disturbance components
u_1, v_1, w_1	longitudinal vortex disturbance amplitudes
p_1	pressure disturbance amplitude
u_1'	secondary instability amplitude
f	secondary instability frequency
t	time
R	radius of curvature for the model surface
$G=\frac{U_\infty \delta}{\nu}\sqrt{\frac{\delta}{R}}$	stability or Görtler parameter
$K=\frac{U_\infty \lambda}{\nu}\sqrt{\frac{\lambda}{R}}$	curve of constant wavelength in the stability diagram
$v_B = \lvert v_B \rvert$	bubble velocity
Δt	time between two exposures during photographing of bubbles
$\Delta s = \lvert \Delta s \rvert$	length of the path covered by a bubble in the time between two exposures
M	scale of reproduction
λ	logitudinal vortex wavelength
$\alpha=\frac{2\pi}{\lambda}$	wave number
β	excitation quantity
δ	boundary layer thickness
θ	momentum thickness

ν	kinematic viscosity
Θ	hot wire excess temperature
x_s, y_s	bubble probe locations
x_{HD-S}, y_{HD-S}	hot wire probe locations
G_s or G_{HD-S}	stability parameter at the locations of a bubble or hot wire probe

EXPERIMENTAL STUDY OF THE LAMINAR-TURBULENT TRANSITION OF A CONCAVE WALL IN A PARALLEL FLOW

H. Bippes
Institute for Applied Mathematics and Mechanics, German Aeronautics and Aerospace Center for Research and Testing, Freiburg, West Germany

Summary /106*

The instability of the laminar boundary layer flow along a concave wall was studied experimentally. Detailed observations of these three-dimensional boundary layer phenomena were made using the hydrogen-bubble visualization technique. With the application of stereo-photogrammetric methods in the air-water system it was possible to investigate the flow processes qualitatively and quantitatively. In the case of a concave wall of sufficient curvature, a primary instability occurs first in the form of Görtler vortices with wavelengths depending upon the boundary layer thickness and the wall curvature. At the onset the amplification rate is in agreement with the linear theory. Later, during the non-linear amplification stage, periodic spanwise vorticity concentrations develop in the low velocity region between the longitudinal vortices. Then a meandering motion of the longitudinal vortex streets subsequently ensues, ultimately leading to turbulence.

1. Introduction

In previous studies it has been shown that before becoming turbulent, laminar boundary layers first assume an unstable state. Randomly occurring small disturbances then become more and more strongly excited downstream until they finally bring about the breakdown of the original flow pattern -- the laminar-turbulent transition. While the initial stagees of this development are still largely within the reach of theoretical treatment, it /107 becomes more and more difficult to describe the subsequent development theoretically the closer one approaches the transition.

Now the purpose of this work is to make an empirical contribution to the further clarification of this problem, using the special case of a concave wall in a parallel flow. This example ahs already been treated several times. The findings obtained up to now show that in contrast to what occurs on flat walls, on a concave wall a three-dimensional instability in the form of counter-rotating pairs of longitudinal vortices with axes in the direction of flow develop and thus confirm the theoretical statement by H. Görtler [1] in this regard. In the literature

---

* Numbers in the margin indicate pagination in the foreign text.

these vortices are referred to as Taylor-Görtler vortices or also as Görtler vortices. In addition, there are also periodic spanwise vorticity concentrations, similar to Tollmien-Schlichting waves, which produce the turbulence in the flat boundary layers in the course of their two-dimensional and non-linear development.

In contrast to the previous studies, a special objective of this work will be to observe the development of Görtler vortices isolated as much as possible from the Tollmien-Schlichting waves. It is hoped to be able to explain what effect Görtler vortices exert on the transition, or whether the transition isn't reduced as it is in the case of flat walls. Moreover, an effort is made, along with a few comparisons of the theory, to also find incentives for expanding the solution equations.

In the experiments the flow is made visible with the hydrogen-bubble method and it is photographed with a photogrammetric stereocamera. In this way it is possible to correctly recognize and interpret the three-dimensional events. The stereo photographs are also analyzed photogrammetrically in order to be able to make quantitative statements. In this way it is possible to indicate the magnitude and direction of the velocity at a specific point.

2. The Stability of the Boundary Layer Along a Concave Wall

2.1 Results of Theoretical Studies

The special feature of flows along curved walls is the occurrence of the centrifugal force as an impressed external force. In the boundary layer on concave walls it decreases from the outer margin of the boundary layer towards the wall with radii of curvature $R >> \delta$ corresponding to the distribution of the main flow velocity U_0, which in this case is equivalent to a circumferential velocity. If in the resulting force field a particle is deflected by a disturbance from its equilibrium position towards the inner or outer edge of the boundary layer, then it reaches zones of lesser or greater centrifugal force and /108
in each case its movement is reinforced (see [2]). G.I. Taylor [3] was the first to study the stability of such a flow both theoretically and experimentally using the example of concentrically rotating cylinders. In so doing, he found that starting with a certain number characteristic for the problem the Couette flow in the gap between the two cylinders became unstable compared with flows in the form of counter-rotating vortex pairs with axes in the circumferential direction.

A similar result was obtained by H. Görtler [1] for the flow next to a concave wall. Fig. 1 gives the disturbance equation as it was inserted into the Navier-Stokes equations

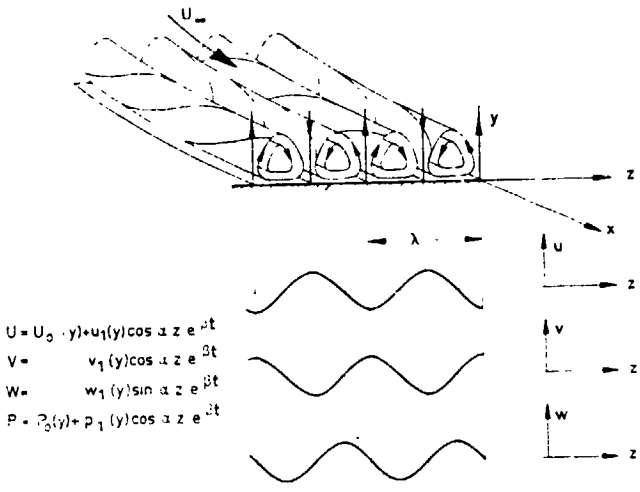

Fig. 1. The longitudinal vortex disturbance.

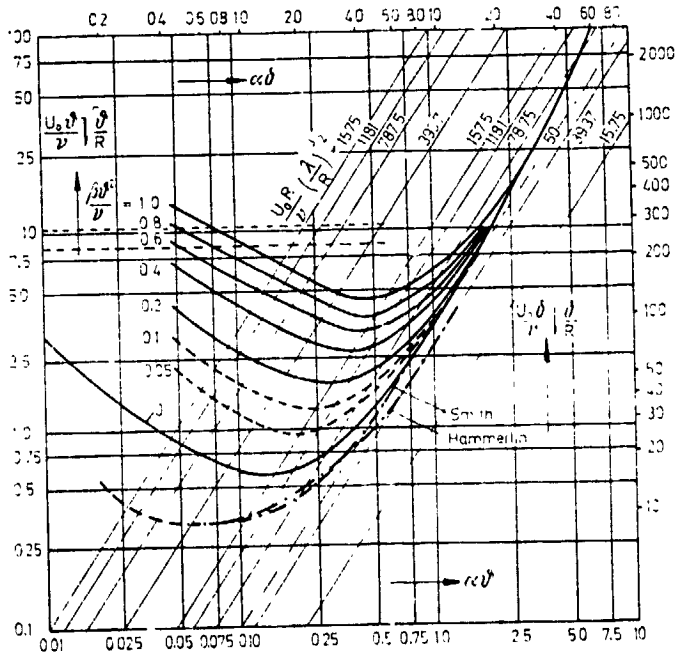

Fig. 2. Stability diagram according to [1] with the neutral curves according to [2] and [5].

in [1]. Here U_0 (y) stands for the main flow velocity and u_1 (y)cosαz, v_1(y)cosαz and w_1(y)sinαz are the components of the perturbed motion. The factor $e^{\beta t}$ specifies its excitation over time. The figure also shows the sketch of the assumed vortex disturbance and the distribution of its components in the span direction. The system of equations obtained after linearization with respect to the small disturbances leads to the eigenvalue problem. The results of the approximate solution given in [1] are contained in the stability diagram shown in Fig. 2. From this it can be seen above which stability parameter

$$G = \frac{U_1 \vartheta}{\nu} \sqrt{\frac{\vartheta}{R}}$$

taken as an eigenvalue the boundary layer becomes unstable in the face /109 of longitudinal vortices of a certain wavelength $\alpha\vartheta$ and to what extent these are excited. The curves of constant excitation

$$\left(\beta \frac{\vartheta^2}{\nu} = \text{const.}\right)$$

can be regarded as valid as long as the assumptions necessary for linearization are observed. Görtler's results were confirmed by a rigorous solution of the same eigenvalue problem by G. Hämmerlin [4], [5]. The neutral curve found in these articles is also plotted in the stability diagram in Fig. 2.

Using a different approach, A.M.O. Smith [2] made a solution equation for the same boundary

layer problem, by, among other things, allowing an outer flow dependent on x and a boundary layer thickness dependent on x. Moreover, he assumed flows which, unlike those of Görtler [1] and Hämmerlin [4], [5] did not develop over time, but developed downstream, i.e. along the path. Thus the results of his approximation solution can be compared with those of Görtler and Hämmerlin only with respect to the neutral curve where the disturbances are neither damped nor excited. Such a comparison, however, shows good agreement especially with Hämmperlin's calculation. As a stability parameter Smith introduces the value $\int\beta dx$ (with β again a measure for the degree of excitation of the vortex disturbance), however he points out that for the special case of constant curvature and constant outer flow the parameter introduced by Görtler is also suitable for describing the stability condition. Smith's solution equation comes especially close to the physical event in an experiment, since here too the boundary layer and the instability increase downstream, i.e. in the x direction. To be sure, the eigenfunctions approximately determined with a Galerkin method to some extent show a purely mathematically determined abnormal behavior so that comparisons with the experiment are not automatically possible. /110

2.2 Results of Previous Experimental Studies

Before the theoretical work of Görtler [1] was known, M. and F. Clauser [6] in their experiments on flat and curved walls, had already found that the laminar boundary layer on a concave wall becomes turbulent at smaller Re numbers than on flat and convex walls. Their findings were later confirmed by experiments by H. W. Liepmann [7], [8]. These were done after the publication of [1] on the same, somewhat improved wind tunnel. Liepmann found a relationship between the critical Reynolds number and the radius of curvature, i.e. he showed that the Görtler parameter G gives a good description of the stability conditions of the boundary layer on a concave wall. Another important result was the confirmation of the finding made by Görtler in his calculations in [1] that, in contrast to concave boundary layers, with flat boundary layers a pressure gradient in the direction of flow exerts only a small effect on the stability. Using the Blasius boundary layer profile, if one converts the Re numbers found by M. and F Clauser for the transition point into a critical Görtler parameter, than this gives values of about 8.5 and 10.5 as against about 6, which is the value found by Liepmann for a similar degree of turbulence in the outer flow, and a value of about 9 for a smaller degree of turbulence. With this comparison it must be borne in mind that the transition point was defined differently in the two experiments. The relationship found by Liepmann between the critical Görtler parameter and the degree of turbulence of the outer flow corresponds to the result which was also obtained

for the flat boundary layer. In the event that the initial disturbances can be regarded as small as defined by the linear theory, still the transition mechanism will always remain the same. For this reason it was also decided in the present experiments not to assign the transition a certain Gortler parameter. /111

While in their hot-wire measurements in wind tunnels the experimenters mentioned so far detected the existence of Görtler instability only indirectly by its effect on the start of the transition, this was made visible for the first time by N. Gregory and W.S. Walker [9] using the tinging method on a Griffith airfoil. Similar pictures were published later by Y. Aihara [10] and I. Tani and J. Sakagami [11]. These visualized the flow with colored liquid or with smoke threads. In so doing, of course, they obtained only general photographs which do not allow more exact interpretation. Their visualization experiments were only intended to supplement more thorough hot-wire measurements.

Through these hot-wire measurements Y. Aihara [10] and I. Tani [12] found that three-dimensional disturbances with a periodicity in the span direction form in the unstable laminar boundary layer next to a concave wall and develop in accordance with the linearized theory up to a certain degree of excitation. The same assertion was arrived at by F. X. Wortmann [13] on the basis of his experiments in a water tunnel with a curved working section. He overlapped periodic three-dimensional disturbances of a certain wavelength in the outer flow by means of a series of rhombic air foils in the span direction and he visualized their development in the boundary layer using Wortmann's method. This work by Wortmann was the first boundary layer visualization study to be carried out on a concave wall, and together with its continuation [14], it is also the only such work to have been done up to this time.

In the absence of a non-linear theory only experiment can provide us with information on the manner in which the turbulence is finally produced further downstream from the described vortex disturbance. According to Aihara [10] and Tani and Aihara [15] the Görtler vortices exert only an indirect effect, specifically by deforming the three-dimensional velocity fields so that velocity profiles of varying stability form along the span. This modifies the already present Tollmien-Schlichting waves to disturbance forms which in flat boundary layers precede the laminar-turbulent transition.

By contrast, in his visualization studies Wortmann [14] found a secondary instability following the Görtler vortices. The former are distinguished from the latter by inclined interfaces between the vortex strands and stationary velocity profiles

with two inflection points. Ultimately the turbulence is brought to a three-dimensional oscillatory motion by means of a third-order instability.

2.3 Aims of these Experiments and their Relationship to Previous Studies

/112

Even if F.X. Wortmann [14], in contrast to I. Tani and Y. Aihara [15], did not go into the effect of Tollmien-Schlichting waves, it is certainly clear that the boundary layer on a concave wall becomes unstable at some time or another in the face of these disturbances. As a result of this, the events which lead to the turbulence will to a certain extent resemble those on a flat wall, especially when the model curvature is so small as in the experiments of Wortmann [13], [14] (radius of curvature R = 20 m) and also by Tani and co-workers [10], [11], [12], [15] (R = 3.5, 5 and 10 m; for a model which was also available with R = 1 m the only test result published was the wavelength of the longitudinal vortex disturbance). To illustrate this, in the graph in Fig. 3 for a few radii of curvature we have plotted the distances x from the leading edge starting at which the laminar boundary layer becomes unstable with respect to Görtler vortices according to the linear theory (G = 0.6) and at which they become turbulent (G = 9) based on experiments by Liepmann [7], [8]. From the stability limit for Tollmien-Schlichting waves which is also plotted it is obvious that the critical curves for both types of disturbance are farther apart, the greater the curvature of the model wall.

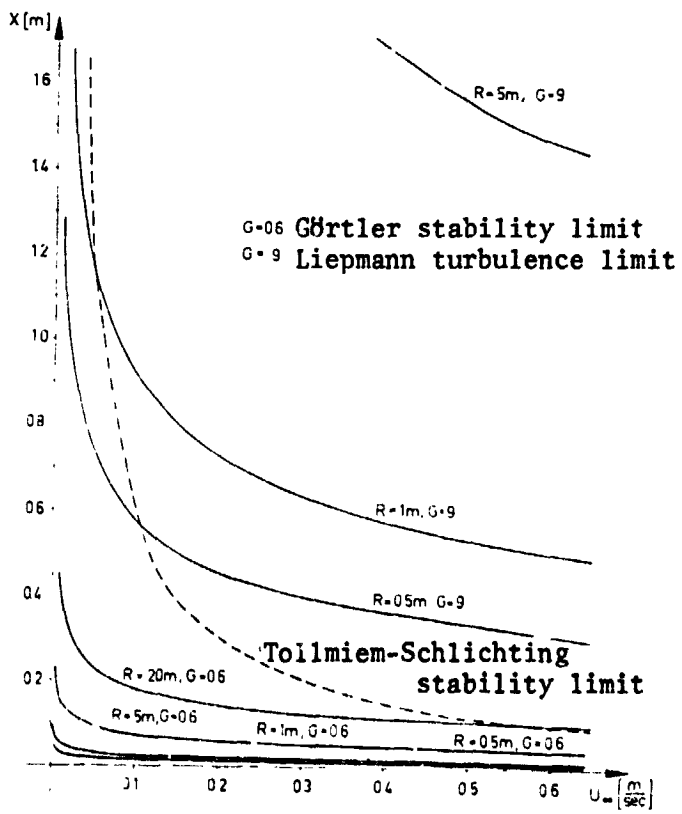

Fig. 3. Stability limits for Görtler vorticies and Tollmien-Schlichting waves and the start of transition found experimentally by Liepmann [8].

The experiments done by the author should therefore supplement earlier experiments insofar as this time models were used which are curved so severely that it is possible to study the development of Görtler vortices and their involvement in the transition process isolated as much as possible from other disturbances, i.e. provided that the flow is still stable with respect to Tollmien-Schlichting waves. For this reason it was also decided not to force periodic disturbances, for example

by means of an oscillating band (Tani and co-workers) or by means of an airfoil effecting rotary oscillations (Wortmann). The experiments were carried out mainly on two models with radiis of curvature of 0.5 and 1 m and working sections of 0.55 and 0.75 m. According to Fig. 3, this seems that in the case of the first model the laminar-turbulent transition can even occur before the boundary layer, according to the linear theory for a flat wall, becomes unstable with respect to Tollmien-Schlichting waves. The same is also true for the second model (R = 1 m) if disturbance generators are used, since these, just like a higher degree of turbulence, reduce the transition limit.

In contrast to previous experiments, a further task of this study was seen to be that of measuring the disturbance components in the direction of the span and perpendicular to the wall in order to complete the picture of the three-dimensional instability and the comparison with the linear theory. Since Wortmann [13] /113
determined a point in the vicinity of the horizontal branch of the neutral curve calculated by Görtler [1] (see stability diagram, Fig. 2), in these experiments too the existence of a right branch should be shown experimentally. Finally, we will also go into detail on the natural wavelength of the disturbances and their effect on the excitation. Tani and co-workers found that the wavelength of the longitudinal vortices is determined by the particular edge effects of the experimental apparatus and less by the curvature of the model or the velocity of the oncoming flow as would have to be the case according to the linear theory.

3. Test Setup

3.1 Water Towing Tank /114

To perform the experiments a water towing tank was set up. Based on comparative studies and taking into consideration the space available, such a test arrangement proved to be the best solution for economically carrying stability experiments in a low-turbulent flow. Among other things, in designing the setup we took into consideration the practical knowledge obtained by Douglas Aircraft Co. [16] and the University of Maryland [17] in operating with smaller towing tanks.

Fig. 4 shows a diagram of the water towing tank built at this institute. The important parts of the tank are the water tank itself (1) and the rail track (3) with the towing car (2). The model, which is immersed into the water, is rigidly attached to the towing car. The intended flow is created when the model is moved in the direction of the arrow by the towing car. The tank itself is a steel frame construction consisting of 4 units connected in series. The bottom and sides of the tank are covered in part with sheets of glass and in part with steel plate for reasons of cost. The two are interchangeable so that /115

Deep cellar Longitudinal section

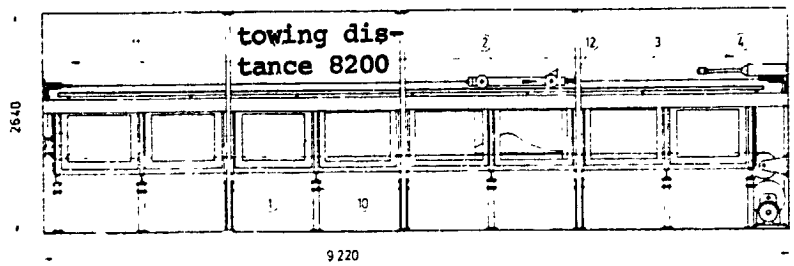

Deep cellar cross-section

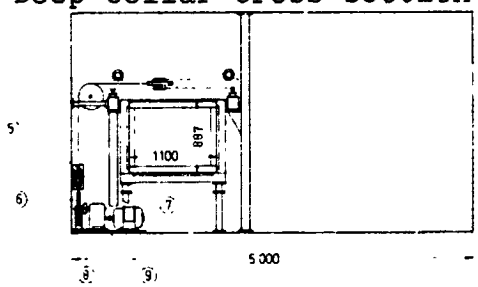

Water towing tank cross-section

Fig. 4. Water towing tank.

1. water tank
2. tow car for model, with model
3. rail track
4. air cushion
5. guide pulleys
6. driving wheel
7. electric motor
8. electric magneto coupling
9. gear unit
10. vibration damper
11. towing cable
12. turnbuckle

it is possible to observe the visualized flow events at any location even though it was not possible to glaze the entire tank. The useable towing length for the experiments was 8.2 m. If necessary, it could be increased by adding additional units. The inside cross-section of the tank, i.e. height and width, was 0.9 x 1.1 m. In order to isolate the flow medium from mechnaical vibrations and to distribute the bearing load as uniformly as possible on all of the feet the entire tank was supported on deformable vibration-damping elements (10).

The rail track was set up completely separate from the water tank so that possible vibrations, for example in connection with the start-up process, would not be transmitted to the flow medium. The car is carried smoothly over the entire distance on two unjointed crane rails. In addition, the bearing surfaces of the rails for the wheels and the guide pulleys on the side were machined. To prevent bending they are mounted on extremely stiff rectangular tubes by means of setscrews at 60-cm intervals. At the same time these also allow the horizontal position to be adjusted.

Motive power is provided a d.c. shunt motor (7). This is also mounted separately from the tank so that vibrations emanating from it cannot affect the water. The power is transmitted to the towing car by means of a drive wheel (6) and an endless tow line (11). The motor speed can be set continuously between 0 and 1500 rpm. Depending on the selection of the diameter of the drive wheel and the inserted gear unit (9) tow velocities or oncoming flow velocities of up to 5 meters per second can be achieved. For a model length of 1 meter this is equivalent to Reynolds numbers of up to $Re = 5 \times 10^6$. Special attention was paid to maintaining a constant oncoming flow velocity. For this purpose the motor speed was set at the desired value with an electronic thyristor control. The control accuracy, with respect to the rated speed of 1500 rpm, is less than 0.2%. With speeds which differ sharply from the rated value the accuracy of course becomes smaller, however with a 4-stage gear unit between the motor and the driving wheel it is always possible to operate in the favorable speed range.

Some idea of the uniformity of the towing speed can be gotten from the photograph shown in Fig. 5. This shows the signals from a hot-wire probe, drawn by the towing car through the still water, displayed on a 4-channel cathode ray oscillograph with two sweeps. The lowest line was drawn for a still probe, i.e. at a tow velocity of $U_\infty = 0$; thus it represents the zero line. The second line from the bottom, compared with the zero /116 line, indicates the changes in voltage over time in the resistance bridge diagonal which makes itself felt at a tow velocity of $U_\infty = 0.075$ m/s. The voltage sweep and time sweep selected for these two traces were 100 mV/cm and 200 ms/cm respectivly. Because of the 10 fold increase in scale in each case (10 mV/cm and 20 ms/cm) and the a.c. input, the two upper lines show the voltage and velocity fluctuations around the mean value. Again the mean value. Again the second line from the top, like the lowest line, was photographed for a nonmoving probe in completely still water ($U_\infty = 0$ m/s). The fact that it deviates from a straightline curve is due to the hum voltage in the hot-wire apparatus. The a.c. trace on top, photographed during the movement of the car, does not show any larger variations compared with the trace photographed at rest, i.e. the changes in voltage caused by the changes in velocity lie within the hum voltage of the hot-wire

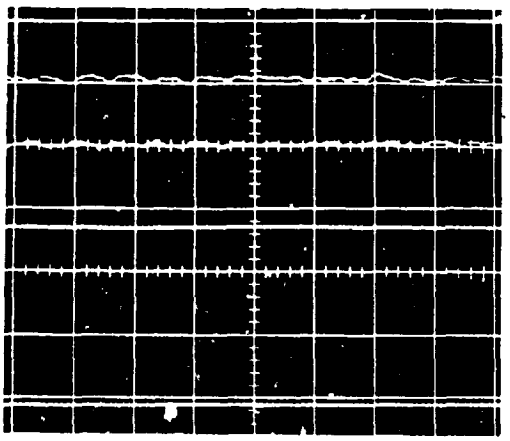

Fig. 5. Hot-wire measurement of the towing velocity.

apparatus. Consequently, they must be less than 0.3%. So far it has not been possible to make a more exact determination with the hot-wire apparatus which is still in the development stage. Nevertheless, these oscillograms also show that the oncoming flow velocity achieved during towing is sufficiently uniform for the stability studies in question.

In order to utilize as much as possible the available tank length for the experiment, i.e. in order to have steady conditions over a sufficiently long path, the drive motor is provided with a rated power of 7.7 kW. This power is sufficient to bring the /117
tow car up to the specified final velocity at the latest after one meter with an acceleration which can be preselected. Braking is accomplished pneumatically by running up against the air cushion (4). By adjusting the air pressure in the pressure cylinders of the cushion designed to absorb the shock it is possible to limit the braking distance to about 0.5 meters for all velocities. Thus the path along which the model can be towed at a constant velocity is sufficient for creating steady flow conditions on the model provided that the model itself is no longer than 2.5 meters.

3.2 Models

Three models were constructed for the experiments with radii of curvature of 5 m, 1 m and 0.5 m. The first was used only for preliminary experiments in order to determine the effect of the amount of wall curvature on the development of the instabilities. It will therefore not be described any further. The two remaining models were built according to the same plan (Fig. 6). The material chosen was transparent plexiglass 8 mm thick.

The concave curvature begins at the leading edge and ends at the tangentially adjoining NACA 2415 profile. The leading edge is wedge-shaped (wedge angle = 15°) and is slightly rounded at the tip (radius = 0.5 mm). Preliminary experiments showed that in this case the stagnation point developed stably. The /118
pressure side is formed from a flat plate which can also be used on its own as a model. Therefore it is possible under the same test conditions to carryout comparative experiments on a flat boundary layer and a concave boundary layer. The models were also sealed on the sides by a flat plate so that as a first approximation a two dimensional flow occurs. Again the leading edges of these side planes are wedge-shaped. A second wall can be introduced equidistant to the curved wall being studied (dotted line in Fig. 6) in case it is desired to eliminate the pressure gradient in the flow direction. The differences produced by this between the pressure above and below the intermediate wall were compensated for as much as possible by screens attached behind the model until the leading edge of the model wall was in a parallel flow. A plexiglass sled was carried along above the model.

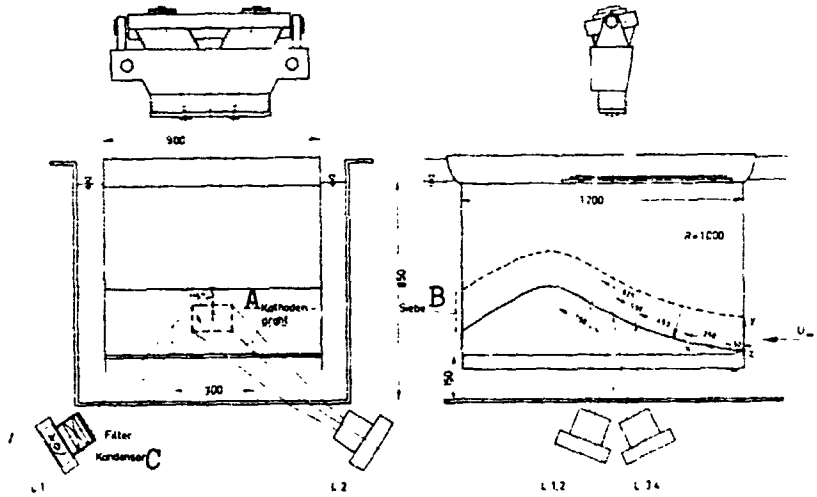

photography arrangement

Fig. 6. Model and photography arrangement
Key: A) cathode wire
B) screens
C) condensor

It is immersed a few millimeters into the water and smooths out any wave motions which may arise on the surface of the water during the towing process which would interfer with the photography. In order to avoid even the slightest optical distortions in the photographs the plexiglass of the sled in the path of the camera was replaced by ground polished plate glass of a thickness of 6 mm.

In order to visualize the flow using the hydrogen bubble method (section 4.1) bubble-producing "horizontal probes" were provided at various places perpendicular to the oncoming flow and parallel to the curved wall. The actual locations were at 0.05 m, 0.25 m, 0.45 m, 0.55 m and 0.625 m downstream from the leading edge. Each of the bubble wires was soldered to two 0.05 mm thick brass pins protruding from the surface of the model. Seen in the span direction these pins are separated by a distance of /119
0.3 m. The distance of the wires form the surface can be varied between 0 and 20 mm so that the flow can be visualized in each boundary layer level. In order to study the oncoming flow (Fig. 7) and get a certain qualitative idea of the velocity profiles with a strongly disturbed boundary layer (e.g. Fig. 44) "vertical probes" perpendicular to the surface of the model were also used to a limited extent. At this point it should be pointed out, however, that the pictures obtained in this way might lead to

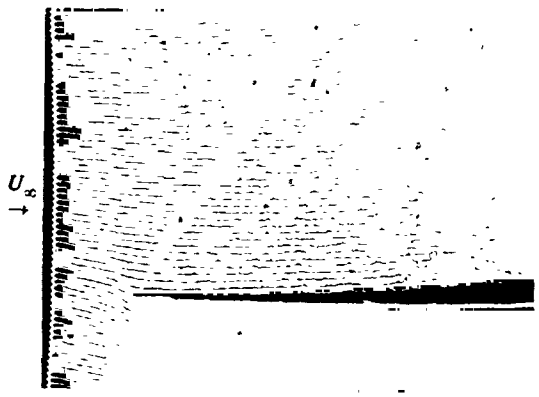

Fig. 7. Flow around the leading edge at U_∞ =0.15 m/s.

false interpretations unless they are photographed and view stereoscopically.

4. Measurement Technique

4.1 Hydrogen Bubble Measurement

As already mentioned, the hydrogen bubble method was used to visualize the boundary layer flow. This method consists of producing hydrogen by electrolyzing the water with a wire-shaped cathode 0.015-0.03 mm thick. This hydrogen, in the form of bubbles 0.01-0.02 mm thick, is carried along by the flow. If these bubbles are illuminated with a beam of light they reflect the rays striking their spherical surface below a certain angle and become visible. In this way it is possible to observe and photograph them on their path with the flow. Within certain limits this path is identical to that of the adjacent fluid particles.

For the experiments done here the hydrogen bubble method has the following advantages:

1. If platinum is chosen as the material for the cathode wires then these are not used up.

2. If very thin wires are chosen for the cathodes then the boundary layer is only slightly disturbed. At velocities around 0.1 m/s, like those occurring in the experiments, the Reynolds number formed with the wire diameter is Re ≈ 2, i.e. no vortex streets yet form in the wake of the wire.

3. Soon after they are produced the gas bubbles dissolve in the water, as a result of which the contents of the tank is always self-cleaning.

4. The hydrogen bubbles can be identified individually in the photographs. This is crucial if one wants to analyze the photographs quantitatively using photogrammetric methods.

Particular aspects of the hydrogen bubble method are discussed in detail in [16], [18], [19] and [20]. In particular, the extent to which the bubble velocity and the flow velocity coincide was studied in [19] and [20]. /120

4.1.1 Streaklines and Timelines

In order to come as close as possible to the goal of producing flow patterns the bubbles here were produced in two ways.

1. A sawtooth-shaped cathode wire was used (Fig. 8 a and b).

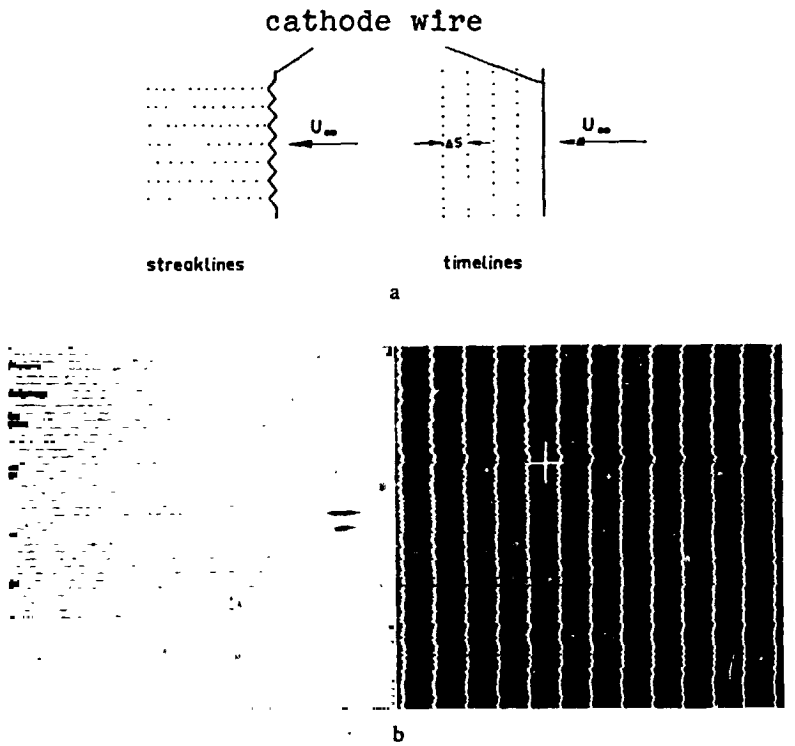

Fig. 8 a and b. a. Schematic diagram of the creation of streaklines and timelines. b. An undisturbed laminar boundary layer flow visualized by streaklines and timelines.

With such a wire the bubbles forming along the entire wire first of all go towards the ends pointing in the direction of flow before they are carried away. The resulting bubble lines are generally referred to as streaklines. In the case of steady flows they are identical with the flowlines. In the case of unsteady flows the streakline patterns, as explained in [20], /121 are very difficult to interpret.

2. A straight cathode wire was used with a pulsating voltage applied to it. As a result the bubbles are not produced continuously, but rather bubblelines are formed at certain

intervals which in general are referred to as timelines (Fig. 8 a and b).

In the case of steady flows the flow velocity can be determined from timeline photographs using the following equation:

$$v_B = \frac{\Delta s}{\Delta t} \qquad \begin{array}{l} \Delta s = \text{distance between two timelines} \\ \frac{1}{\Delta t} = \text{pulse frequency} \end{array} \qquad (4.1)$$

In the case of nonsteady flows, in which the bubbles emanating from a certain point on the wire no longer take the same path all of the time, one will get an error in v_B by using the above equation. The greater the distance of the bubble from its point of origin, the greater will be the error (cf. [20]).

A considerable improvement can be achieved if the photographs can be twice exposed for a brief time within a certain interval. Thus in this way the timelines are photographed twice and with Δs the path can be determined which has been covered by one and the same bubble in Δt, the time between two exposures. The bubble velocity v_B to be formed in turn from Eq. (4.1) in this case contain only an error due to averaging over the time interval Δt which, however, can always be selected very small. Consequently the measurement must no longer be restricted to points in the vicinity of the prove where, moreover, the accuracy is reduced by the velocity defects in the wake of the probe (also see section 4.3).

4.1.2 Power Supply for Producing the Hydrogen Bubbles

For electrolyzing the water, i.e. producing the hydrogen bubbles, a power supply unit was used which delivers a d.c. voltage which can be set between 0 and 600 V at a maximum current of 5 amps. These ranges are sufficient in order to control the current for producing the hydrogen in such a way that the number of bubbles coming off the cathode wire is sufficient at any possible towing velocity to visualize the flow.

As described in section 4.1, in order to form timelines the bubble current coming from the power unit was periodically switched on and off by a thyristor switch (see block diagram in Fig. 9) in regular, sharply delineated time intervals. As a result, sharply delineated bubble lines cleanly separated from the cathode wire were produced in an appropriate manner. Since quantitative picture analysis requires exact knowledge of the time interval Δt (section 4.1, Eq. (4.1)) between the creation of the individual timelines, a crystal stabilized timing generator /122

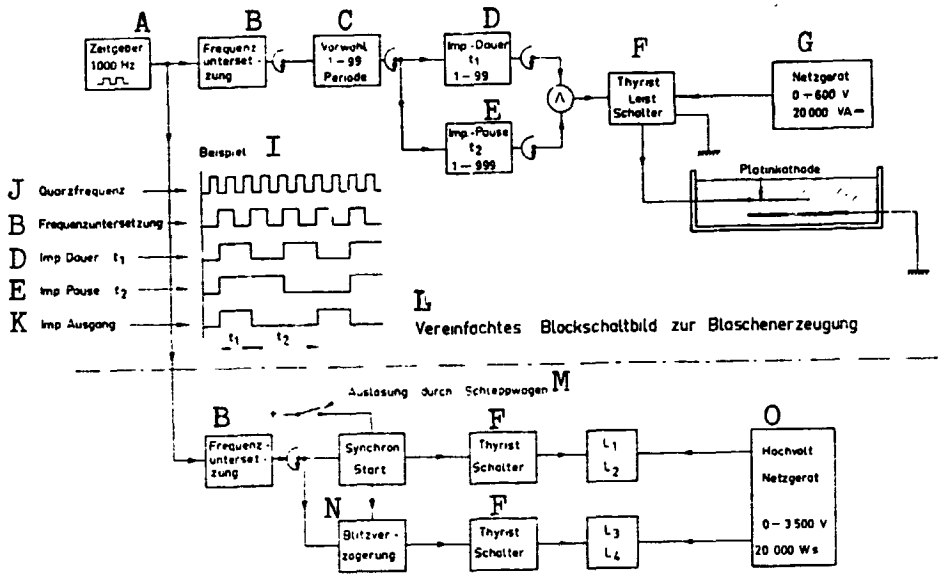

Simplified block diagram for charging flash bulbs.

Fig. 9. Block diagram of the power supply for producing the hydrogen bubbles and for charging and igniting the flash bulbs.

Key: A) timing generator
B) frequency division
C) preselection period
D) pulse duration
E) pulse interval
F) thyristor switch
G) power supply
H) platinum electrode
I) example
J) quartz frequency
K) pulse output
L) simplified block diagram for bubble production
M) triggering by tow car
N) flash delay
O) high voltage power supply

was used to control the thyristor switch. Starting at a basic frequency of 1,000 Hz, with this apparatus it was possible to select a pulse duration or gate-controlled rise time in a range of 0.001-0.099 s and a pulse interval in a range of 0.001-0.0999 s by adding integral multiples of 0.001 s for the basic oscillation period. Moreover, by means of a binary frequency division it is possible to expand all of the times even more by factors of 2^1, 2^2,..., 2^{11}. The deviation of the crystal stablized basic frequency from its ideal value (1,000 Hz) is less than 0.05%. Since with the thyristor switch only a little of this high degree of accuracy is lost and thus the switching times are specified to an accuracy of at least 10^{-6}s, the error in Δt is never greater than 1%.

4.1.3 Illumination /123

Xenon flash lamps (E.G. & G. Inc., model FX-77 C4) were used for illumination. With a discharge time of 0.3 ms these can be loaded with about 4,000 Ws. This high energy is necessary because the white light occurring during the flash discharge must be filtered out with the exception of a narrow frequency band in order to avoid unsharp photographs due to color dispersion. The latter results during refraction of the light rays on the surface of the water or of the sled (Fig. 6 p. 11). The Schott filter used here was transparent for light rays of wavelengths over 510 nm. Since the spectral sensitivity of the plate emulsion used (Agfa Gevaert 23D56) ended at about 560 nm, the photographically effective light which remained was only that of the narrow frequency band between 510 and 560 nm. In turn, only the small portion of this reached the camera which struck the surface of the bubbles at an angle less than the angle of total reflection. The movement blur of the object (bubble) was kept sufficiently small by the briefness of the flash discharge.

Lamps were set up on both sides of the tank to achieve uniform illumination of the flow field covered by the camera (Fig. 6, p. 11). To produce the twice exposed photographs the pairs of lamps L1-L2 and L3-L4 were ignited sequentially at an interval of Δt (also see section 4.1). The ignition process was initiated by the tow car running over a terminal contact (bottom diagram in Fig. 9). Whereas the ignition pulse for L_1-L_2 occurred immeidately, the one for L_3-L_4 was delayed by a preset interval Δt. The timing is controlled by the same principle described above for producing the timelines. Delay time could be chosen in integer multiples from 0.001 to 0.999 ms. In addition, each of these time could in turn be expanded by factors of 2^1, 2^2, 2^3 or 2^4. Because of the thyristor control of the ingition pulse it was possible to specify the selected values for t to an accuracy of at least 1%. A high voltage power supply was built to feed the flash lamps. When using 4 lamps at the maximum discharge voltage up to 6,000 Ws per lamp and per discharge could be delivered. The shortness of the discharge time was achieved by means of the low-induction design and the very small resistances in the circuit connections and feed lines.[1]

For photographs with a stationary camera the flash lamps were replaced by water-cooled high pressure mercury vapor lamps (SP 1000 W). With these lamps the light emanated from a luminous surface measuring 10 x 12.4 mm. In order to pick up as much of /124 this as possible and focus it in a narrow beam onto the object

---

1. The necessary equipment and the circuitry for producing the bubbles and the flash illumination were developed by Pavle-Čolak-Antić, Ph.D. Eng. and A. Maier, Eng. (also see DVL-Nachrichten, vol. 38, 421-422 (1969)).

the lamps were installed in slide projectors (Leitz-Prado with Hektor 1:2.8/300 mm). Air-cooled high perssure mercury vapor lamps (HBO 500 W) were used for photographs taken by the camera which travelled with the model. They were likewise installed in slide projectors (Leitz-Prado with Elmaron 1:2.8/150 mm). These were attached to the side of the tow car and were carried along just like the camera.

4.1.4 Photography

The first experiments showed (see section 5.1) that the instabilities occurring on the concave wall have a pronounced three-dimensional character. Therefore it seemed essential to produce stereophotographs which would allow sufficiently precise qualitative and quantitative picture analysis. For this purpose a photogrammetric stereocamera (i.e. a camera in which the position of the perspective center is known with respect to the image plane) was built for taking close-up photographs, taking into consideration the special photograph conditions existing here. (For details on the construction see section 4.2.2.) The objectives used were nearness-corrected Apo-Ronars (1:9/240 mm) made by Rodenstock. These are standard repro objectives with a compur shutter. Synchronous exposure in both parts of the camera was guaranteed by flashing with the shutter open in the dark room. Of the available negative emulsions that of the Scientia 23D56 by Afga Gevaert proved to be the best for bubble photographs. With sufficient sensitivity (approx. 10 DIN) and strong contrast ($\gamma \approx 2.2$) it offers sufficient fineness of grain (165 lines per mm). For reasons of maintaining accuracy during development and the best possible flatness in the image plane, glass plates had to be used to hold the emulsion. In order to record the dynamic transition events 16 mm photographs were made with a Bolex H 16 M camera (objectives: Cine-Xenon 1:2/50 mm and Switar 1:1.9/75 mm) and with Scientia 50B65 (20 DIN, $\gamma = 1.2$; 120 lines/mm) by Agfa-Gevaert.

4.2 Velocity Measurement Using Photogrammetric Analysis of Hydrogen Bubble Photographs

In order to measure the flow velocities a method was introduece here which is based on visualizing the flow with hydrogen bubbles and determining the movement of these bubbles during a time Δt by photogrammetric ananlysis of stereophotographs. The bubble velocities found in this way are compared with the local flow velocity. In comparison with the usual methods for measuring velocity, this method requires a considerable amount of work, for the location of the individual bubbles in the photograph must always be carefully measured with respect to a photograph coordinate system before one can calculate the position in space. Moreover, with the photographs made in these experiments the image-forming rays of light emanating from the bubbles are refracted at

/125

the surface of the water before they reach the camera which is situated in the air. In such a "two-medium case" it is no longer possible to use the usual evaluation mehthods which are based on the creation of a pattern. One must have recourse to less practical analytical methods involving large amounts of numbers.

However in contrast to point measuring hot-wire probes, pitot tubes etc., the velocity measuring method described here has the decisive advantage that in the analysis one has a view of the events in a large section of the flow field. As a result, one recognizes the the striking points and can make the measurements precisely at those points. Thus from the outset one avoids the difficulty of finding a coherent picture of the flow from measured values which were obtained at various points. Furthermore, it should be borne in mind that with this method the magnitude and direction of the velocity is determined. This is especially valuable in the study of three-dimensional flow fields.

The possibility of quantitatively analyzing simple flow photographs has already been utilized before ([13], [19] and [20]), however no photogrammetric methods were used. In addition, because of the restriction to single-photograph measuring, it had to be assumed that all of the observed particles moved in a plane parallel to the surface of the water, the image plane and the perspective plane, hence an assumption which cannot be fulfilled with a curved model or anywhere where three-dimensional flow phenomena occur. In order to verify this, the distance from the wall of the bubbles in a time line was determined photogrammetrically using a stereophotograph of the laminar boundary layer flow disturbed by Görtler vortices (see section 4.2). The result is shown in Fig. 10. Fig. 27 (p. 37) shows a partial

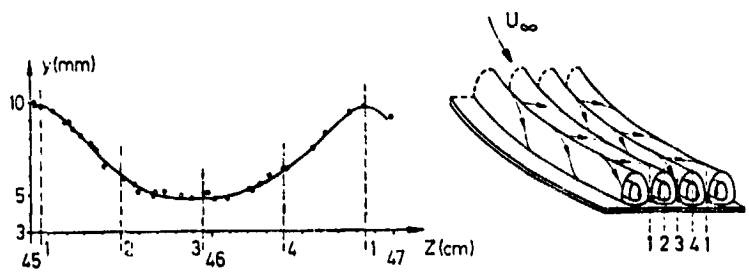

Fig. 10. Distance from the wall y, measured photogrammetrically, for the time line indicated by the arrow in Fig. 27, plotted over the span direction z. The distances measured from the wall can be coordinated with the corresponding points z in the longitudinal vortex disturbance by the numbers 1, 2, 3 and 4.

picture of the photograph used (photography arrangement shown in Fig. 6, p. 11). The measured timeline there is indicated by an

arrow. It is obvious from the result that the bubbles, which emanate from a probe parallel to the wall, are located 5 to 7 cm downstream from the wall in very different boundary layer levels. If with this example, as in the case of single-photograph measuring, it were necessary to assume that the bubbles were always moving in the plane parallel to the wall and containing the probe, then one would assign false velocities to the actual distance from the wall. /126

4.2.1 Photogrammetry in a Two-Medium System

As already mentioned, in the two-medium case it is no longer possible to analyze the stereometric photographs in the conventional way using the optical approach to produce a model of the path of the rays since there are no two-medium evaluation instruments necessary for this. With one-medium evaluation instruments the refracting surface is missing. If one uses these instruments for two-medium photographs, then as K. Rinner [21] has shown, the projecting beams emanating from a pair of picture points in general no longer intersect in a suitable object point. Even stereoscopic analysis is no longer possible where the rays go by together at a greater distance from the wall (also see [22]). Nevertheless, in order to be able to use conventional evaluation methods, K. Rinner [21] and G.C. Tewinkel [23] have suggested optical compensation methods. Such methods, however, cannot be used if as in this case the distance in air and the distance in water of the object distance are in a ratio of 2:3. Even the method suggested in [22] of approximately calculating the actual position of the object point from the apparent position obtained using conventional evaluation instruments is not used with the water depths occurring here, since an "apparent position" cannot be found for all points. Therefore in this case there remains only the numerically involved method of calculating the position of the points in space from the individually measured pairs of picture points using the general imaging equations.

Fig. 11 shows a schematic diagram of the optical path of rays in a two-medium system. O_1[1] and O_2 are the centers of perspectivity (perspective centers of the objectives) and B_1 and B_2 are the two image planes in the camera (B_1 is drawn in the diapositive position and B_2 is left out of the drawing); π is the refracting surface. The space point P is represented by the projection beam with the main rays $x_B - x_E - q$ in image point P'. α_1 and β_1 are the directions of the object to be photographed before and after refraction. If one knows the position of the two cameras in a fixed three-dimensional coordinate systems and also the position of the refracting surface ("external orientation"), /127

---

1. The symbols for the photogrammetric variables are defined in this section and do not appear in the notation list.

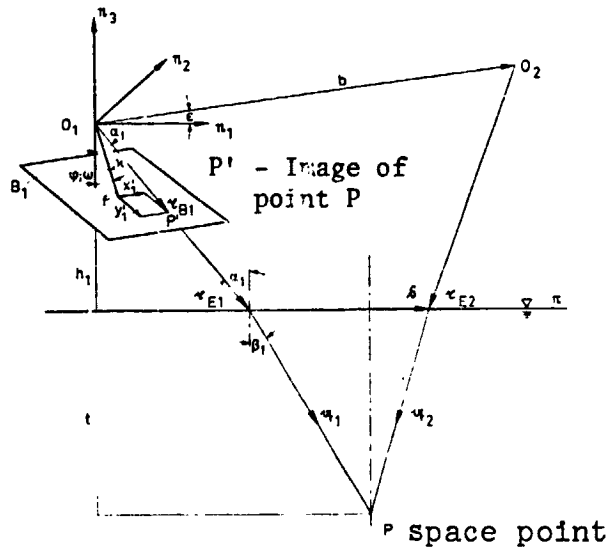

Fig. 11. Optical path of rays in a two-dimensional system.

then the original position in space of the object points can be determined from the image point positions indicated in the two-dimensional image coordinate system by using simple three-dimensional intersections.

$$x_{E1}+q_1=b+x_{E2}+q_2. \qquad (4.2)$$

Obviously a precondition here is that for the cameras the position of the centers of perspectivity is known with respect to the image plane ("inner orientation").

For a mathematical solution to the orientation problem one can proceed in the following way using the approach of K. Rinner [21]:

First of all a model of the path of rays in the photographs is set up by determining the outer orientation. This can be done using the following orientation variables:

$$\omega_1;\varphi_1;\kappa_1 \quad \text{and} \quad \omega_2;\varphi_2;\kappa_2,$$

stand for the angles for each three rotations of the two cameras; v is the ratio of the base b to the height h, and ε is the angle of inclination of the base with respect to the horizontal. The model is then fit into a fixed three-dimensional coordinate system in correct scale. In addition, the size of the base, a scale factor and the planimetric position of the recording point for one camera must be determined.

If the vectors in Eq. (4.2) are replaced by the orientation variables mentioned above and by the coordinates of the points reproduced in both cameras, then from this can be found the 8 unknowns for setting up the model if at least 8 pairs of image points in a stereophotograph are available in the two-dimensional image coordinate system. One then has to solve a system of 8 irrational transcendental equations. The four unknowns for adjusting the model can be determined in a simple way from the planimetric position of two "control points" or from the position in space of one control point and a planimetric coordinate of another. (Control points are object points whose position in space in known in a fixed 3-dimensional coordinate system.)

An iterative approximation method is used here to solve the orientation problem. The introduction of 10-16 control points makes possible a compensation method for minimizing the sums of squares of the differences between the photogrammetrically determined spatial positions of the control points and their actual position in space.[1]

4.2.2 Photogrammetric Stereocamera Design

Construction of a special camera proved to be necessary for two reasons. It had to be designed for extremely close-up photographs (scale of reproduction 1:1.5 to 1:2) in order to reproduce the small light-reflecting portion of the hydrogen bubbles measuring about 0.02 mm so that these could be identified and measured on the pairs of pictures. In addition, they had to be constructed in such a way that for optical and computing purposes the best approximate perpendicular photographs could be produced even under the existing photographic conditions. for this reason the camera is mounted so that it is adjustable and can be moved only horizontally in the direction of travel on the towing car. Thus both optical axes a (see Fig. 12) are always perpendicular to the surface of the water. Since the tangential planes on the surface of the model have an increasing slope towards the surface of the water from the leading edge backwards, for reasons of sharpness the image plane must also always be inclined towards the surface of the water for the different photography positions (angle of inclination δ). This is analogous to the Scheimpflug condition in a one-medium system. The simultaneous change in the object distance is compensates for by a change in the image distance. Along with these necessary changes in the inner orientation, the plates along with the plate holders in the image plane can be moved towards one another in the image plane in the direction of the base (see direction of arrows in Fig. 12). Thus completely overlapping pictures can be taken at all photograph positions. The magnitude of the orientation change in each case

/129

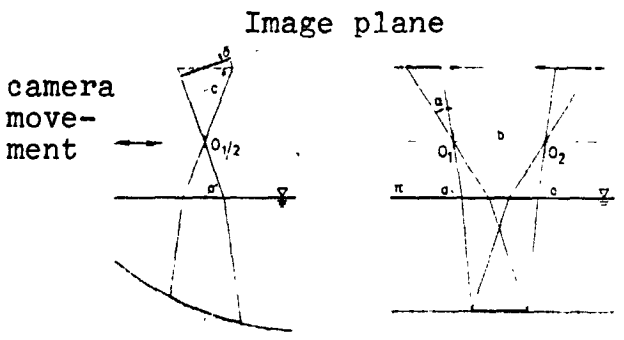

Fig. 12. Diagram of the photographic conditions.

1. The orientation problem using the discussed approximation method was carried out by A. Lehmann, graduate student in mathematics, on a Siemens 2002.

can be read from exact scales. To be sure, this design is based on the principle of using test cameras with a fixed inner orientation for reasons of accuracy, however it must be borne in mind that extreme close-up photographs are to be produced here in which image coordinate errors result in errors in the space point determination which are still in the same order of magnitude.

The initial approximations required for the iterative calculation of the outer orientation can be read off the camera or they are known from the outset, since the optical axes of the two cameras enclosed in one housing are always directed perpendicularly to the surface of the water. Fig. 13 shows the photogrammetric stereo cameras on the towing car.

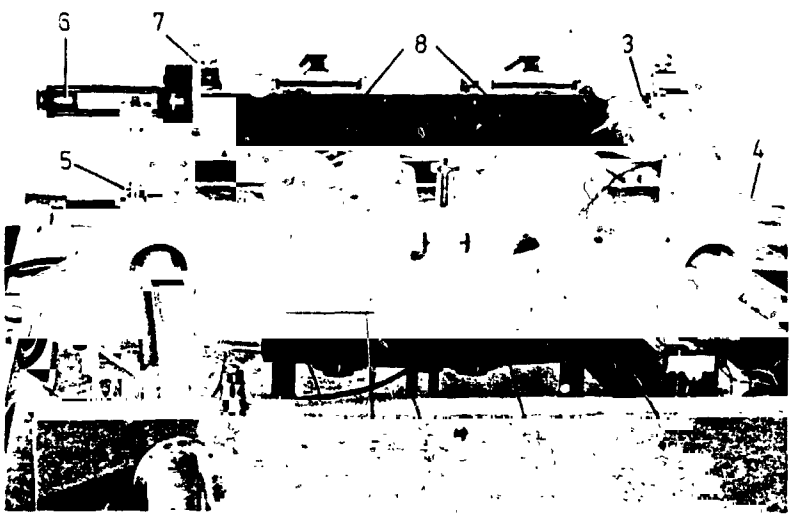

Fig. 13. Photogrammetric stereo camers on the towing car.

The body of the camera (1) with the lens carrier plate (2) which can be moved towards it and the tilting rear portion (3) is attached to two round bars (4) in a fixed frame. The frame is supported on the towing car and can be leveled. By means of this last provision the camera axes can be aligned vertically. Two bubble levels (5) are used to check the levelness of the system (one scale division ≙ 0.01 mm/m). The pivoting angle of the image plane is read with a reading microscope (6) on a glass scale (7) to an accuracy of 0.01°. The location of the principle points on the image can be read on scales (8) to an accuracy of 0.02 mm for each position of the film holder. The distance between the photograph locations and the surface of the water is measured by means of a depth gauge (9) with a micrometer adjustment attached to the camera. To simplify the adjustment of the cameras and the

/130

calculation of the orientation, both cameras are mounted in a rigid housing with a common principle image plane and principle plane of the lens. This firmly predetermines their position with respect to one another, i.e. the relevant orientation variables are known with respect to one another. The number of unknowns is decreased from 8 to 6.

Camera information:

base	b = 250, 185 or 120 mm
image distance	c = 400-310 mm
pivot angle	δ = 0-17°
objectives	Apo-Ronare 1:9/240 mm
negative material	9 x 12 plates or roll film and 70 mm film in Linhol film holders.

4.2.3 Picture Coordinate Measurement /131

Since there was no commercial stereocomparator available for measuring the pictures, the picture measuring instrument shown in Fig. 14 had to be constructed. With this instrument the picture point coordinates can be measured to an accuracy of 0.005 mm in a room with maximum temperature variations of 2°C. The coordinate adjustment was calibrated with contact copies of a grid plate made by the Wild Co. With the x-parallax adjustment screw (1) it is possible in principle to make stereoscopic measurements. This facilitates the identification of correlated points on the two partial pictures. To be sure, for the reasons discussed in [22] this cannot be done in most cases with the two-dimensional photographs made in these experiments.

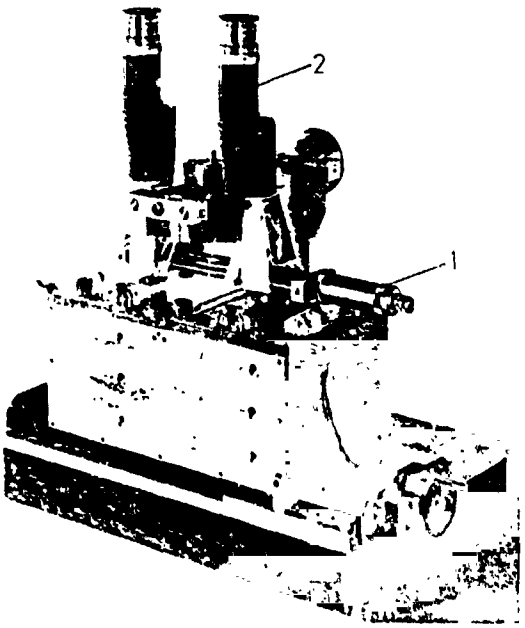

Fig. 14. Picture measuring instrument.

To increase the accuracy of measurement the pictures were examined through a stereomicroscope (2) with a magnifying power of 30 X. However, since this takes in a section of the picture measuring only 7 mm in diameter, the prism stereoscope shown in

STANDARD TITLE PAGE

1. Report No. NASA TM-75243	2. Government Accession No.	3. Recipient's Catalog No.
4. Title and Subtitle EXPERIMENTAL STUDY OF THE LAMINAR-TURBULENT TRANSITION ON A CONCAVE WALL IN A PARALLEL FLOW		5. Report Date March 1978 6. Performing Organization Code
7. Author(s) H. Bippes, Freiburg, W. Germany Institute for Applied Mathematics and Mechanics, German Aeronautics and Aerospace Center for Research and Testing,		8. Performing Organization Report No. 10. Work Unit No.
9. Performing Organization Name and Address Leo Kanner Associates Redwood City, California 94063		11. Contract or Grant No. NASw-2790 13. Type of Report and Period Covered Translation
12. Sponsoring Agency Name and Address National Aeronautics and Space Administration, Washington, D.C. 20546		14. Sponsoring Agency Code

15. Supplementary Notes

Translation of "Experimentelle Untersuchung des laminar-turbulenten Umschlags an einer parallel angeströmten konkaven Wand," Heidelberger Akademie der Wissenschaften, Matematisch-naturwissenschaftliche klasse, Sitzungsberichte, no. 3, 1972, pp. 103-180.

(A73-22450)

16. Abstract

The instability of the laminar boundary layer flow along a concave wall was studied experimentally. Detailed observations of these three-dimensional boundary layer phenomena were made using the hydrogen-bubble visualization technique. With the application of stereo-photogrammetric methods in the air-water system it was possible to investigate the flow processes qualitatively and quantitatively. In the case of a concave wall of sufficient curvature, a primary instability occurs first in the form of Görtler vortices with wave lengths depending upon the boundary layer thickness and the wall curvature. At the onset the amplification rate is in agreement with the linear theory. Later, during the non-linear amplification stage, periodic spanwise vorticity concentrations develop in the low velocity region between the longitudinal vortices. Then a meandering motion of the longitudinal vortex streets subsequently ensues, leading to turbulence.

17. Key Words (Selected by Author(s))	18. Distribution Statement
	Unclassified-Unlimited

19. Security Classif. (of this report)	20. Security Classif. (of this page)	21. No. of Pages	22. Price
Unclassified	Unclassified	68	

NASA-HQ

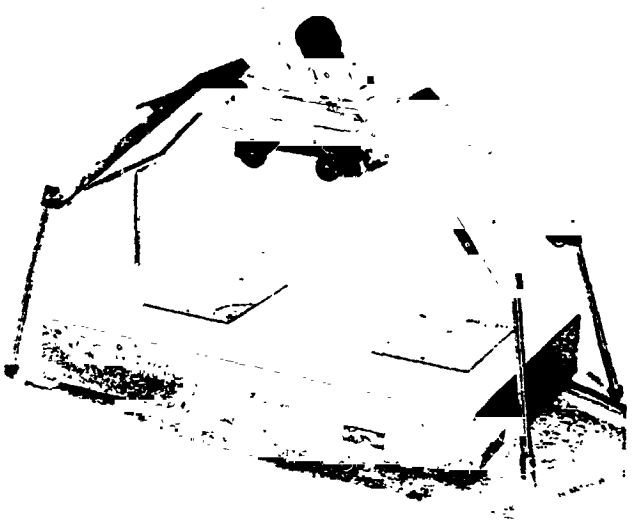

Fig. 15. Prism stereoscope made by Tokoyo Optical Co. Ltd.

Fig. 15 can be used to get an overall view of the entire flow pattern recorded in the picture. It can be used at magnifications of 1.5 X, 3.5 X and 6 X.

4.2.4 Accuracy of Measurement /132

As was shown in section 4.1.1, the velocity of flow can be determined from the following equation:

$$v_B = \frac{\Delta s}{\Delta t} \qquad (4.1)[\text{sic}]$$

The value obtained from this is first of all subjected to pure measurement errors in Δs and Δt which arise in the photogrammetric evaluation and in the measurement of the time between two exposures. In addition, however, there are also all of the errors which result from the fact that because of the effect of various forces the bubbles do not exactly assume the velocity of the surrounding particles of fluid. In particular, the following errors occur:

1. Errors in the photogrammetric evaluation. To begin with, if one assumes that the data of the inner and outer orientation are known, then the accuracy of the photogrammetric measurement depends essentially on the error in the picture coordinate measurement. With respect to the connection here the reader is referred to an estimate given in [44], p. 140 ff., for the normal case in a one-medium system. In a first approximation it can also be used for perpendicular photographs in a two-dimensional system. In this case the additional inclination of the image plane by the angle δ (see Fig. 9) can be allowed for by using /133 the following equation for the image distance:

$$c = c + y\cos\delta \qquad (4.3)$$

Thus it is also true in this case that picture measuring errors affect primarily the height determination (three-dimensional coordinate Z, see Fig. 16) according to the following relationship:

$$|dZ| \approx \frac{Z^2}{bc} d(x' - x''). \qquad (4.4)$$

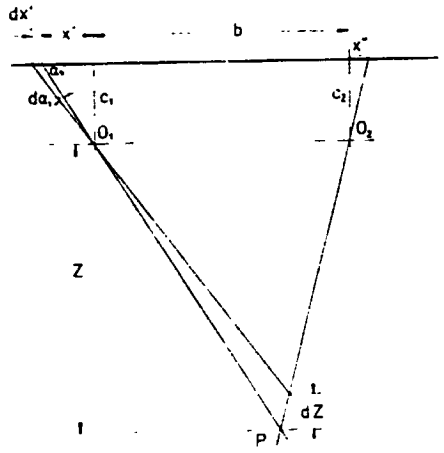

Fig. 16. Diagram for estimating photogrammetric error.

Accordingly, the error |dZ| increases quadratically with Z. This means that close-up photographs, such as were made in these experiments (scale of reproduction Z/c = 1.5-2) can be evaluated substantially more precisely than "air pictures" with Z/c > 6,000, or alternatively, larger tolerances can be permitted with respect to the picture measuring instrument and the inner orientation of the measurement camera. As further follows from Eq. (4.4), to utilize the achievable accuracy the base must be selected as large as possible, i.e. until image angles α occur for which the objectives are just still corrected. In the photographs made here the base ratio was b/Z ≈ 1/4.

If one substitutes the following numerical values from a flow photograph made in these experiments in Eq. (4.4) b = 185 mm, Z = 650 mm (converted to an equivalent distance in air) and c = 380 mm, and allows for the fact that, given the grain of the plate emulsion used, the picture coordinates can be measured to an accuracy of 0.01 mm with the picture measuring instrument shown in Fig. 14, then with $d(x'-x'') \leq 0.1\sqrt{2}$ we obtain variations for Z of /134

$$dZ \leq 0.14 \text{ mm}$$

The variations estimated up to that point can be increased further by errors in the orientation data. In order to avoid this an effort was made to keep the orientation errors as small as possible so that they could be ignored with respect to the picture measurement errors.

With the data for the outer orientation this is possible by calculating them anew for each photograph with the help of check points.[1] As for the data for the inner orientation which are introduced as known variables into the calculation, it must be possible to read these on the scales provided (see section 4.2.2) for the camera setting in each case up to a certain maximum

---

1. Marks of a square network scratched onto the model wall were used as checkpoints. The position of these marks with respect to a three-dimensional coordinate system was measured with theodolites to an accuracy of 0.02 mm in the layer and an accuracy of 0.05 mm in depth.

failure. An estimate which was made according to the specifications in [44], page 140 ff., gave the following allowable reading errors: $\Delta c \leq \pm 0.05$ mm for the common image distance (owing to the principle of construction) of the two cameras; $\Delta\delta \leq \pm 0.035°$ for the inclination of the image plane, also common to both cameras because of the principle of construction; and $\Delta x'_h = \Delta x''_h \leq \pm 0.01$ mm for the principle image point coordinates in the direction in which the film holders can be moved.

The relevant accuracies of adjustment are $\Delta c \leq \pm 0.02$ mm; $\Delta\delta \leq \pm 0.01°$ and $\Delta x'_h = \Delta x''_h \leq \pm 0.02$ mm. Thus while with respect to c and δ the calculated allowable errors are not exceeded, this is certainly not achieved at $\Delta x'_h$ and $\Delta x''_h$, but in this case a correction is possible using the check points.

It should also be mentioned that with the calculation method used here for solving the orientation problem it was decided not to likewise introduce the inner orientation variables, since the extent to which the orientation problem can still clearly be solved was not being investigated.

To check the error estimate the spatial coordinates of check points found by photogrammetric evaluation of a stereometric pair of points were compared with the theodolite measurement. The differences are listed in Table 1 along with the corresponding space point coordinates. It turns out that the photogrammetric accuracy of measurement estimated above can be maintained.

TABLE 1. PHOTOGRAMMETRIC DETERMINATION OF CHECK POINTS ON THE FLOW MODEL AND COMPARISON WITH THE THEODOLITE MEASUREMENT /135

point	X [mm]	ΔX [mm]	Y [mm]	ΔY [mm]	Z [mm]	ΔZ [mm]
1	677,71	−0,05	769,42	−0,09	75,94	−0,06
2	727,51	−0,04	768,64	−0,01	75,59	−0,11
3	777,65	−0,06	768,71	−0,02	75,79	−0,09
4	677,39	0,02	815,27	−0,06	95,33	0,15
5	727,54	−0,02	814,89	−0,01	94,97	−0,06
6	777,27	−0,01	814,87	0,07	95,29	−0,00
7	677,06	0,01	860,41	0,06	118,07	0,05
8	727,10	0,00	859,27	−0,11	117,65	0,17
9	777,07	0,00	859,80	0,10	117,71	0,00
10	676,71	0,07	903,78	−0,03	143,44	0,08
11	726,74	−0,01	902,67	0,08	142,99	−0,02
12	676,26	0,09	945,82	−0,01	170,00	−0,06
13	776,49	0,01	945,25	−0,02	169,49	−0,04

According to these considerations the errors arising in the photogrammetric determination of Δs can be stated as follows: if one always chooses Δt, the time between two exposures, so large that the hydrogen bubbles during this time cover a distance of

$\Delta s \geq 3.5$ mm, then the error with respect to this entering into the velocity measurement is:

$$f_{1,1} \leq 4\%$$

2. Averaging error. With Δs as the path of a bubble between two exposures one calculates, using Eq. (4.1) for v_B, the average value over time of a Langrangian velocity. Since in the case of unstable flows such a velocity differs from the Eulerian velocity being sought here, an error is produced which becomes larger as Δs is selected greater. In [20], p. 22 ff., it was estimated to be 1.1% for a turbulent wall boundary layer at $\Delta s \approx 5$ mm. For the path lengths Δs chosen here and in the disturbed laminar flow the following is certainly valid:

$$f_{1,2} < 1.1\%$$

3. Error caused by the wake of the probe wire. As long as the bubbles move in the wake of the probe wire their velocity is correspondingly smaller than outside of the wake. Measurements by V. Graefe [24] have shown that the loss in velocity has faded away after 500 wire diameters at the latest (in this case 12.5 mm). Since in these experiments the measurements were always made at a greater distance from the probe, this error can be ignored, especially since the bubbles, as experiments have shown, emerge from the wake very quickly when the probes are horizontal. /136

4. Error due to the effect of inertia. Because of the large difference in density between water and hydrogen, the time in which the bubbles are accelerated to the speed of the surrounding fluid particles is very brief and can be noticed only in the case of unsteady flows. According to [20], p. 31, this can cause an error of 0.5% in a turbulent wall boundary layer. In the case of a disturbed laminar boundary layer flow the difference will certainly be smaller so that it can be ignored with respect to other errors.

5. Error caused by bubble bouyancy. The bouyancy forces, which also occur because of the difference in density between water and hydrogen, impart to the gas bubbles a characteristic movement in a vertical direction. The final velocity of this motion was determined in [20] to be $v_A = 0.4$ mm/s for a single bubble assuming that $Re_d < 1$ is valid for the Reynolds number formed with the diameter. Our own measurements show that this value in the vicinity of the probe, where the bubbles are always very dense, is always exceeded. At a distance of one to two centimeters downstream from the probe the value is $v_A = 0.4$-0.5 mm/s. Therefore there remains an additional, residual error of less than 0.1 mm/s which cannot be corrected. Thus in measuring velocity components in a vertical direction which are

greater than 0.5 cm/s, the residual error which cannot be corrected is

$$f_{\Delta s_3} < 2\%.$$

6. Error caused by the centrifugal force. Another characteristic movement of the bubbles is produced in a flow field with curved flow lines by the centrifugal force, since depending on the density this acts to a different extent on gas bubbles and the fluid particles surrounding them. If this inertial force is compared with the buoyancy force A, then the following rough estimate is valid for the flow conditions in these experiments ($U < 0.3$ m/s, $R = 1$ m):

$$\frac{Z}{A} = \frac{\frac{\pi}{6} d^3 (\rho_{H_2O} - \rho_{H_2}) \frac{U^2}{R}}{\frac{\pi}{6} d^3 (\rho_{H_2O} - \rho_{H_2}) g} < \frac{U^2}{Rg} < \frac{1}{100}$$

i.e. the characteristic motion due to the effect of centrifugal force can the ignored in this case.

7. Error in Δt. As explained in section 4.1.3, the error in Δt is less than 1‰ and can be ignored.

Total error. Thus only the errors in Δs enter into the calculation of the average quadratic total error in U. If measurements are made with spaces between timelines of $\Delta s > 4$ mm, then /137

$$f_{\Delta s\,ges.} < \sqrt{4^2 + 1{,}1^2 + 2^2} \approx 4{,}5\%.$$

Provided as in this case there is a disturbed laminar boundary layer flow which approximates the steady state, Δs can be selected even greater. The total error then becomes even smaller.

4.3 Disturbance Generators

In an unsteady laminar boundary layer flow the instabilities are formed from incipient disturbances of varying intensity and arbitrary form such as are always present in every flow in a random distribution. Natural disturbances, therefore, appear in differing states of excitation depending on the initial intensity (see Fig. 17). Thus a very irregular flow pattern is formed which is not suitable for a systematic investiageion of the events which lead to the laminar-turbulent transition. One only obtains information on what type of flows they are with respect to which the boundary layer in question first becomes unsteady.

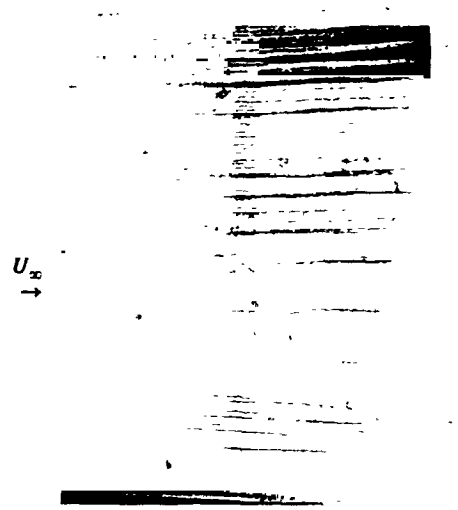

Fig. 17. Natural occurrence of instabilities in an oncoming flow affected by disturbances. R = 0.5 m; U_∞ = 0.1 m/s; G = 5.5 (middle of picture).

Moreover, if the intensity of the initial disturbances is only very small, then the instabilities only become visible or detectable if they are very intensely excited. Their further development up to the laminar-turbulent transition is almost like an explosion (see Fig. 29, p.38), in the process of which it is no longer possible to observe their development in space and time with the available equipment. /138

These obstancles in the way of the intended studies can only be overcome by forcing disturbances in the boundary layer with a uniform distribution and with a sufficient inital intensity, such has been the common practice dating back to G.B. Schubauer and H.K. Skramstadt [25]. As discussed in greater detail in the following sections, screens and heated wires were used as disturbance generators in the experiments described here.

4.3.1 Using Screens to Generate Disturbances

In order to create an isotropic as possible disturbance field cloth screens with uniformly spaced meshes of equal size measuring about 20 cm were mounted in front of the model (see Fig. 18). The Perlon threads were 0.2 mm thick, the mesh size was 0.5 mm (quadratic mesh shape, 2 mm and 4 mm) the latter two being hexagonal mesh shapes. In accordance with [26], disturbances produce behind the screen are damped if a critical Reynolds number, which depends on the aperature ratio of the screen (the ratio of open screen area to total screen area), is not exceeded. This Reynolds number is formed with the thread diameter. For the three screen it is the following: Re_{crit} = 42, 66 and 70 respectively. This means that the velocity of the oncoming flow must remain less than 0.21 m/s, 0.33 m/s and 0.35 m/s so that the wake disturbances behind the screen fade away in isotropic turbulence. In addition, the aperture ratios of the screens used are also large enough (0.59; 0.8; 0.9) to exclude fluctuations in U along the span which could establish the wavelength of the logitudinal vortex disturbance. In fact, in wind tunnel experiments P. Bradshaw [27] measured fluctuations in the boundary layer velocity U in the span direction on flat if screens with an aperture ratio of 0.57 were used in the damping chamber. /139

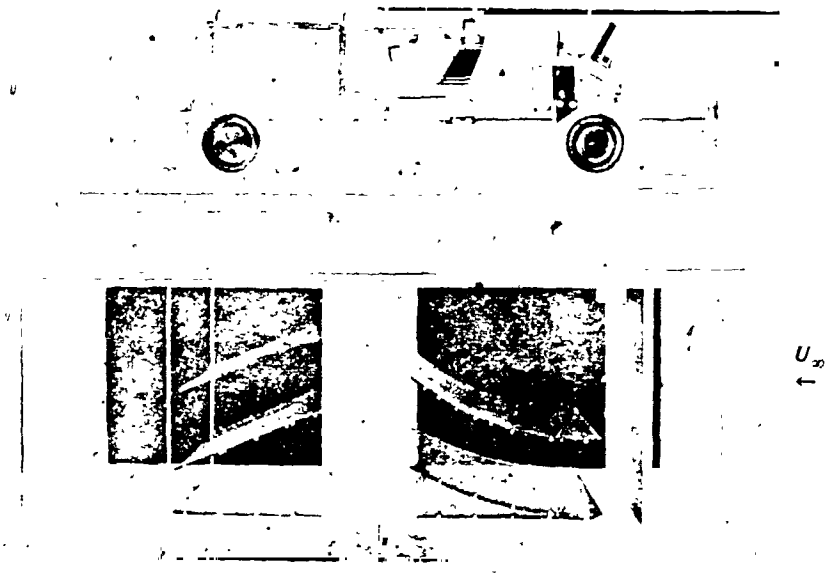

Fig. 18. Model with screen towed in front.

4.3.2 Using Hot Wires to Generate Disturbances

These are a new type of disturbance generator. In experiments without disturbance generators and with screens used to produce disturbances it was found that of all the wide variety of disturbances present in the strongly concave boundary layer (behind the screen), longitudinal vortices of a certain wavelength are always excited first (see section 5.1). This result was utilized in designing this new type of disturbance generator. In order to initiate these logitudinal vortices along the span by means of a small initial pulse, four hot wire coils were inserted close to the leading edge of the model. The coil parts on the concave surface run parallel and in the direction of flow (See Fig. 19). The spacings between the coils correspond to the

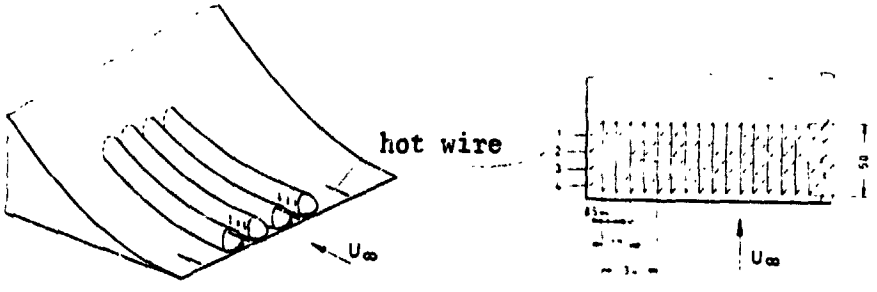

Production of logitudinal vortices over the hot wires

Hot wire coil on the leading edge

Fig. 19. Heated wires used to produce disturbances.

average wavelengths found in the experiments using screens. The sires are produced from a non-oxidizing platinum-rhodium alloy and they have a diameter of 0.1 mm. Their specific resistance is $\rho = 44.6\ \Omega/m$.

When the coils are heated with an alternating current of 50 hZ the particles of fluid in their immediate vicinity are heated and set into motion as a result of the uplift created by the heat. This motion corresponds to the vertical velocity component in the middle of a pair of longitudinal vortices. By heating one, two or all four heating coils, pairs of longitudinal vortices of three different wavelengths can be produced in the unsteady concave boundary layer. These wavelengths are in a ratio of 1:2:4. By this means it is possible to check the effect of the wavelength on excitation. /140

The initial intensity of the disturbances can be varied by the voltage applied to the heating coil. In the experiments it was adjusted in such a way that excess temperatures between 0 and 60°C were produced on the wire depending on the velocity of the oncoming flow.

At $\Theta = 0$ the coil parts of the hot wires lying on the model surface being investigated act only like an individual roughness element. According to [9] and [28], such an element can likewise involve longitudinal vortices provided that the following equation is valid for the Reynolds number calculated from the roughness level K:

$$Re_K = \frac{KU_K}{\nu} > 300\, Re_{krit}$$

(U_K = velocity at the upper end of the roughness element).

In these experiments Re_K always remains smaller than Re_{crit}, but Re_{crit} in [28] was found on a flat plate for a spherical roughness element, while in this case we were dealing with pieces of wire 50 mm long running in the direction of flow. These will certainly cause more intense disturbances. The experiments also then showed that already at velocities of $U_K > 0.6$ m/s or at $Re_K > 60$ vortex pairs emanate from the hot wires like those shown in [9] and [28]. However, velocities as low as $U_\infty > 0.15$ m/s were sufficient to initiate the vortex field created on the concave wall.

In the present experiments it was decided from the outset not to use small airfoils, as has been done many times ([13], [15]) to initiate the longitudinal vortex disturbance predicted theoretically for the unsteady boundary layer on the concave wall. The reason for this was that with such airfoils in addition to the desired edge vortices periodical disturbances are also pro-

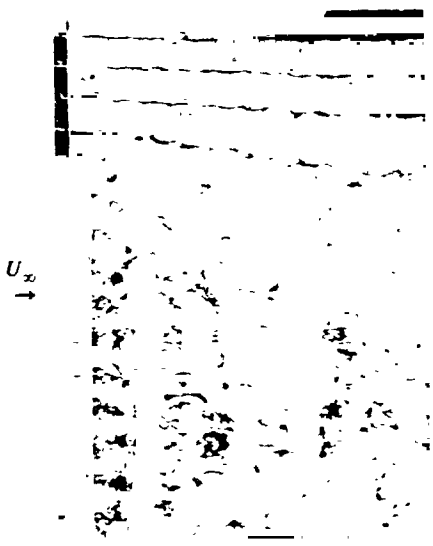

Fig. 20. Streakline photograph of the wake of a 0.3-mm thick airfoil with a depth of 8 mm and a width of 30 mm. U_∞ = 0.4 m/s; Re = 3.2 x 10^3 (calculated using the wing chord as the characteristic length). The view is from above looking at the suction side of the airfoil.

duced at the same time in the wake of the trailing edge (see Fig. 20). To be sure, with respect to these periodic disturbances the concave boundary layer for the model being studied is still stable according to the linearized theory, but with increasing intensity they could nevertheless become active by means of nonlinear coupling effects, for example based on the theoretical model of K. Menzel [29] or J.T. Stuart [30]. /141

5. Experimental Results

5.1 The Instability Occurring in the Boundary Layer on a Concave Wall

To find out what type of instabilities form in the unstable laminar boundary layer flow on a concave wall no interference generators were used to begin with in the experiments. Then an isotropic disturbance field was superimposed on the oncoming flow using the screens described in section 4.3.1. This disturbance field contained the components for all conceivable types of vorticies. This was supposed to show which of these components are excited and to what extent the instabilities arising in the process are equivalent to those which are formed without a screen. Finally, the hot wires (section 4.3.2) were to be used as a disturbance generator which was capable of initiating only the type of instability detected up to that point.

If, as assumed in the theory, counterrotating longitudinal vortex pairs are involved, then streakline and timeline patterns would be created behind horizontal probes like those sketches in Fig. 21 b and c respectively. Depending on whether the probe is above or below the vortex axis (Fig. 21 a), the streakline in those places where the distrubance component v is directed upward and w = 0 will spread out or converge (Fig. 21 b). The timelines will preserve a wave form in which the crest in each case will appear where v is directed towards the wall and w is again 0 (Fig. 21 c). Thus while the disturbance component w in particular can be visualized by streaklines, the timelines reveal the curve of u along the span. Further information on bubble motions /142

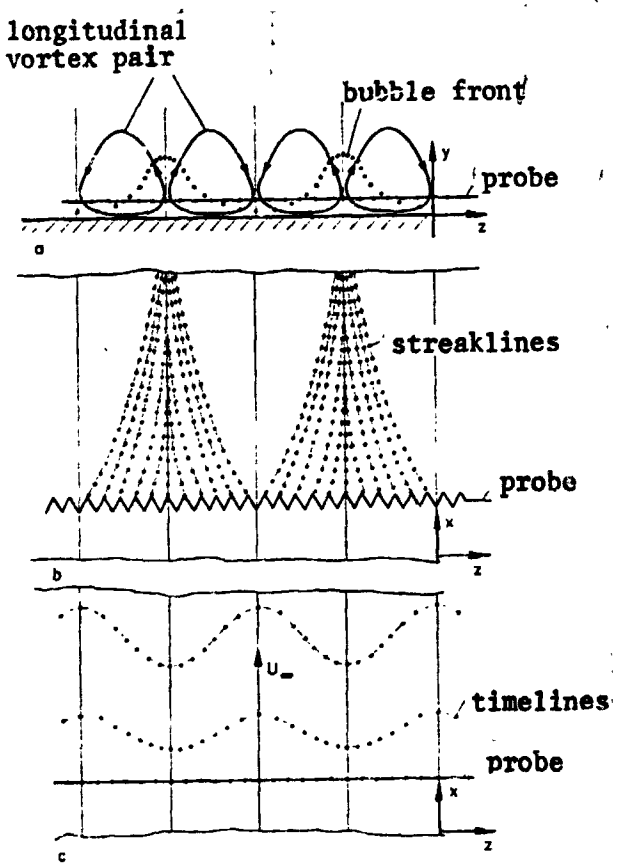

Fig. 21. Streakline and timeline configurations behind horizontal probes in a laminar boundary layer flow disturbed by counterrotating longitudinal vortex pairs.

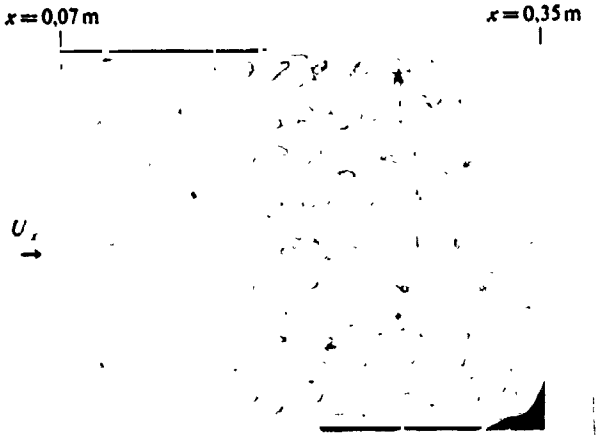

Fig. 22. Streakline photograph of an unstable boundary layer flow without generated disturbances. Model R = 0.5 m; U_∞ = 0.5 m/s; G = 9 (at the transition point); x_S = 0.08 m; $y_S/\delta \approx 0.7$.

can be provided by varying degrees of picture brightness in the photographs. For instance, these are produced if bubbles converge or spread apart and form areas of varying density which correspondingly reflect different quantities of light.

5.1.1 Experiments without a Disturbance Generator

In well damped water (damping time about 1 hour) i.e. with an oncoming flow which is substantially free of disturbance, the instabilities first become visible at Görtler parameters which far exceed the critical value. Beyond this point, however, they become so strongly excited that even after a short distance downstream from here the transition takes place.

Fig. 22 can provide an insight into such flow fields. This is a streakline photograph for which the bubbles were produced intermittently.[1] The bubble front, which to begin with run in a straight line in the span direction, become wave-shaped further downstream. This means that the

1. As with all of the photographs, unless otherwise noted the photography arrangement and view direction of the camera are as shown in Fig. 6, p. 11.

Fig. 23. Streakline photograph of an unstable boundary layer flow without generated disturbances, but with the oncoming flow subject to random disturbances. R = 0.5 m; U_∞ = 0.125 m/s; G_S = 3.84; x_S = 0.2 m; $y_S/\delta \approx 0.3$.

laminar primary flow has been superimposed by a periodic disturbance component u in the z plane. In addition, the greater degree of brightness conspicuous on the wave crests indicates the presence of a periodic disturbance component w also in the z plane.

If this experiment is repeated in water which is not yet completely damped, i.e. if there are randomly distributed disturbances of greater intensity present in the oncoming flow, then those among them which are excited will become visible even at smaller values of G, though in a very irregular formation and at varying intensity, as can be seen in Fig. 23. For this photograph the flow was visualized with streaklines. As a result, the occurrence of the disturbance component w is now indicated directly by the alternatingly decreasing and increasing spaces between the streaklines (cf. Fig. 21 b). /144

5.1.2 Experiments with Screens

A qualitatively similar, but more regular flow pattern is created if the laminar oncoming flow is superimposed by an isotropic flow field produced by towing screens in front of the model of the type described in section 4.3.1. Viewed in the span direction, the streaklines (Fig. 24) again alternately converge and spread apart, in the process of which streaks running in the direction of flow which now clearly have a greater bubble density than before (Fig. 23). Stereophotographs

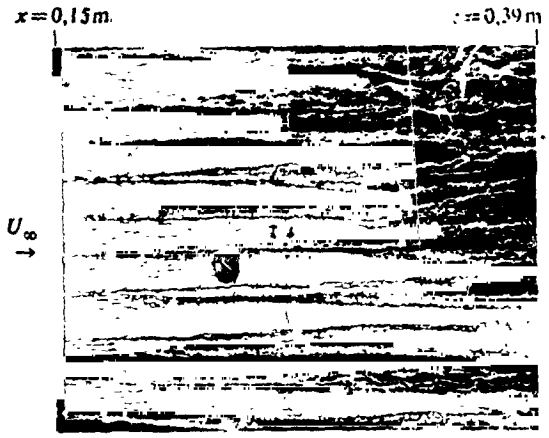

Fig. 24. Streakline photograph of an unstable boundary layer flow with disturbances produced by a screen. R = 0.5m; U_∞ = 0.11 m/s; G = 4; K = 145; x_S = 0.15 m; $y_S/\delta \approx 0.3$.

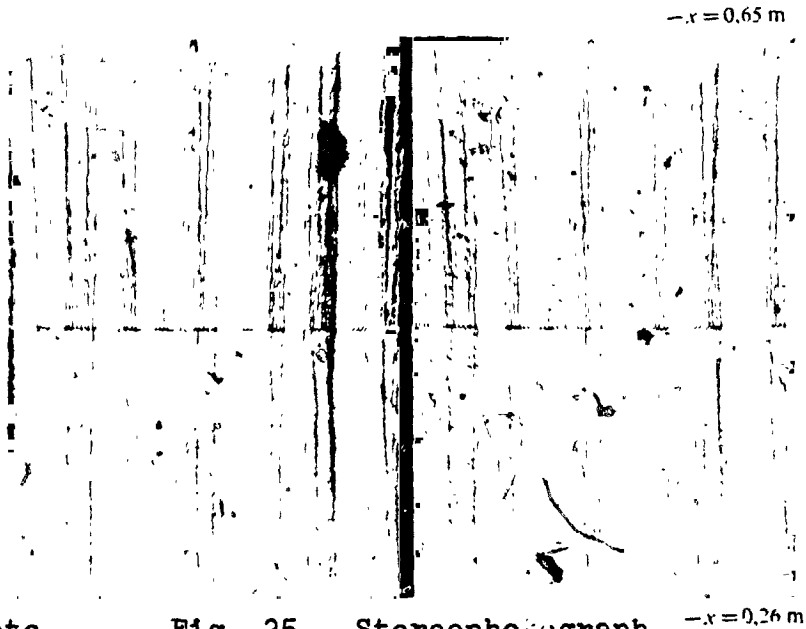

Fig. 25. Stereophotograph of an unstable boundary layer flow with disturbances produced by a screen, visualized by two successive probes. R = 1 m; U_∞ = 0.1 m/s; G = 5.7 at x_{S2}); x_{S1} = 0.25 m; x_{S2} = 0.45 m; $y_{S1}/\delta \approx 0.3$; $y_{S2}/\delta \approx 0.3$.

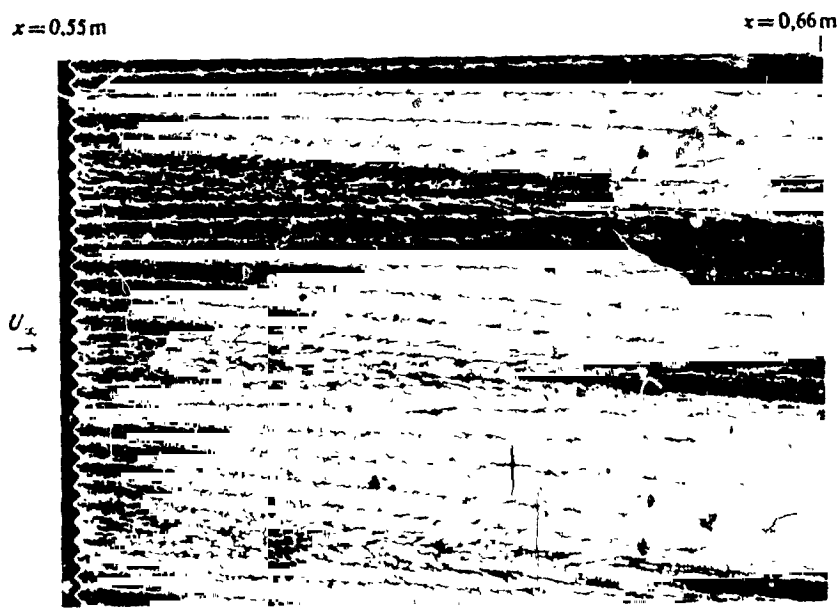

Fig. 26. Streakline photograph of an unstable boundary layer flow with disturbances produced by hot wires. R = 1m; U_∞ = 0.05 m/s; G_S = 5.5; x_S = 0.55m; $y_S/\delta \approx 0.25$.

bubble density than before (Fig. 23). Stereophotographs[1] (see Fig. 25) in which the probe is below the vortex axis as in Fig. 21 show that the bubbles of these longitudinal streaks move upward, while those of the places lying in between move downward. /146

Thus it can be said in summary that, in the boundary layer of the model of unstable laminar primary flow under investigation, excited disturbances u (Fig. 22) v and w (Figs. 23, 24 and 25) are superimposed with a periodicity in z. These are at least similar to those made by the disturbance equations in the linearized theory. It can also be said that out of the entire variety of disturbance components in the oncoming flow only those are excited which contribute to the formation of this three-dimensional instability.

5.1.3 Experiments with Heated Wires

On the basis of this purely qualitative result it was now possible to develop and use the hot wires described in section 4.3.2. To be sure, these excite longitudinal vortices, but otherwise they do not cause any additional other types of disturbances. Streakline and timeline photographs made using hot-wire coils (Figs. 26 and 27) show qualitatively the same instabilities as Figs. 23, 24 and 22, and moreover the flow field has now become sufficiently regular so that reproducible measurements can be carried out. /148

The double exposed time line photograph in Fig. 27 is a partial picture of one of the stereometric pairs which were evaluated according to the method described in section 4.2. An initial result which was obtained in this way is that shown by the curves in Fig. 28 a, b and c for the velocity components $U + u$, v and w along the span direction z at a distance from the wall of $y/\delta \approx 0.5$. With the broken lines labelled 1, 2, 3 and 4 the measured velocity values can be coordinated with the corresponding places in the vortex field diagramed in the upper right hand corner of the figure and with the flow photograph in Fig. 27.

If one compares this result with the solution equation made by Görtler [1] in his stability studies as given in Fig. 1, p.3, then it can also be stated quantitatively that longitudinal vortices develop in the unstable flow condition on the concave

---

1. The stereophotographs can be observed with a pocket stereoscope. The two partial pictures are joined together without any gaps. The pocket stereoscope must be moved in a horizontal and vertical direction in order to be able to observe each section of the pictures.

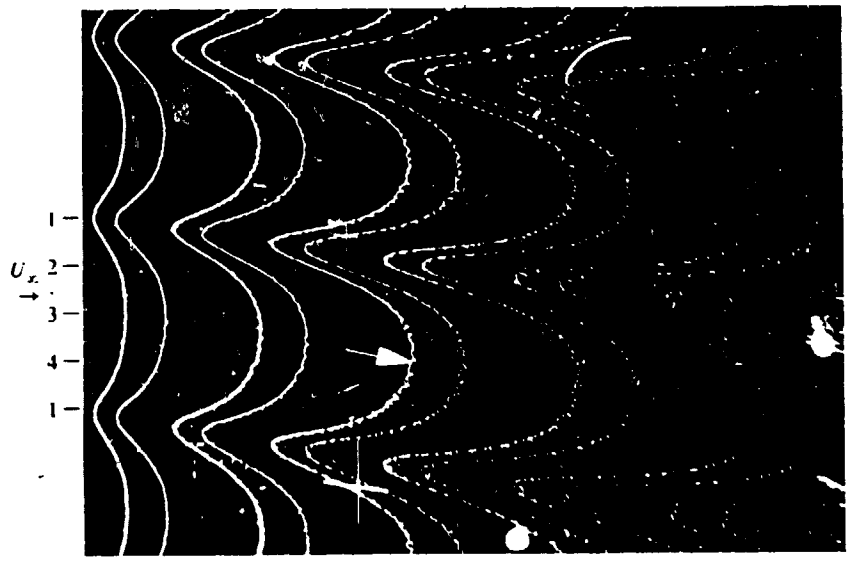

Fig. 27. Double exposed timeline photograph of the flow shown in Fig. 26. Δt = 0.080 s.

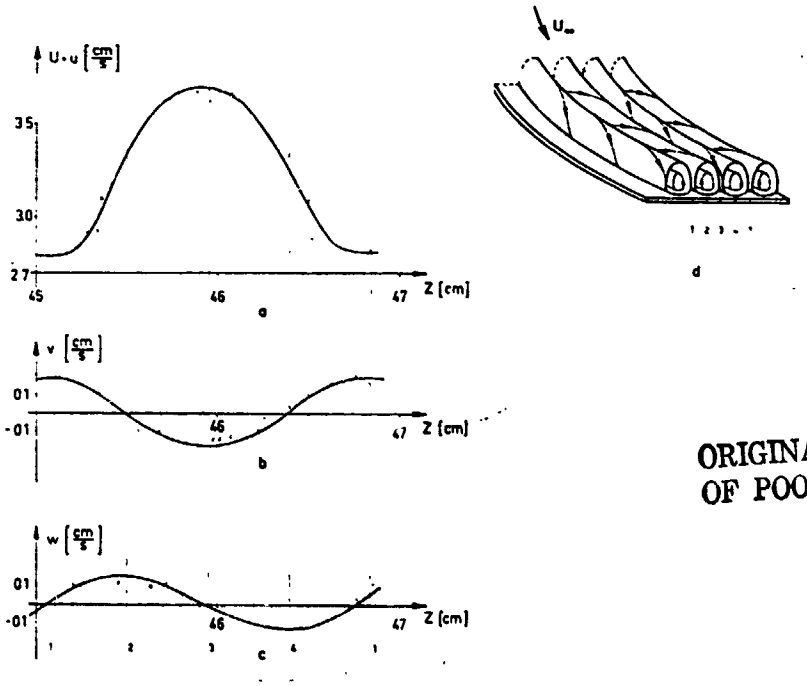

Fig. 28. Result of photogrammetric evaluation of double exposed timeline photographs as shown in Fig. 27. a - velocity component in the oncoming flow direction; b - velocity component perpendicular to the wall; c - velocity component in the span direction; d - diagram of the vortex disturbance.

wall in a parallel flow which have the same shape as those which are possible according to the linearized stability theory.

5.2 Effect of the Wall Curvature

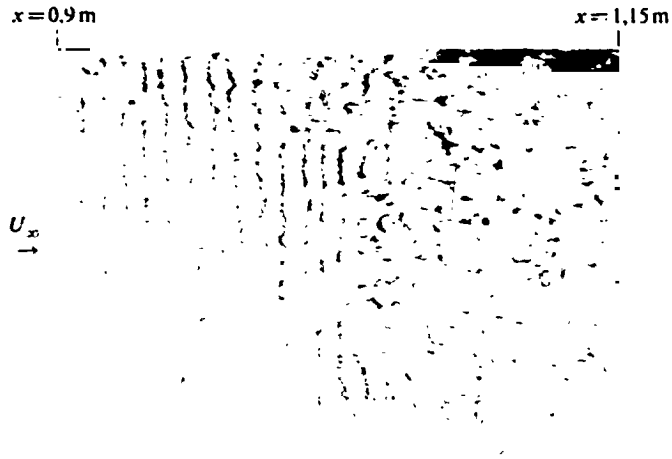

Fig. 29. Laminar-turbulent transition for the model with a radius of R = 5 m. U_∞ = 0.8 m/s; G = 8 (in the transition region); x_S = 0.9 m; $y_S/\delta \approx 0.3$.

The effect of the curvature on the development of the instability was investigated only qualitatively in this work. First of all, a model with a test surface having a curvature with a radius of 5 m was studied without a disturbance generator. In so doing, it turned out (Fig. 29) that the transition proceeded very suddenly (also see section 5.1.1). Instabilities /149 in the form of pronounced longitudinal vortices could not be determined, but rather Tolmien-Schlichting waves, even though the boundary layer according to the linearized theory first b comes unstable with respect to Görtler vortices. Of course, with this small curvature and with the oncoming flow velocity of 0.8 m/s which had to be selected in order to bring the boundary layer to the transition before the end of the concavely curved portion of the model at about x = 1.1 m, the two stability limits are very close together, namely at x = 0.04 m and 0.08 m (Fig. 3, p. 6). In Fig. 29 the occurrence of Tollmien-Schlichting waves is hinted at by the varying spaces between the timelines in the flow direction. These spaces are indeed equal in the undisturbed laminar flow in accordance with how they are produced (see section 4.1.2 and Fig. 8b, p. 13. In contrast to this, the Görtler vortices could clearly be detected without a disturbance generator for the model with the radius of curvature of R = 0.5 m (section 5.1, Fig. 22) and also for the model with R = 1 m although even with this model longitudinal vortices of smaller intensity can be observed. This becomes especially conspicuous during the laminar-turbulent transition, for while the longitudinal vortex streets on the model with a radius of R = 0.5 m still exist even after the transition (Fig. 30), they are already destroyed for the model with a radius of R = 1 m (Fig. 31).

Furthermore it can be observed that on the more strongly /150 curved wall the transition takes place within a shorter distance. Since in this case also the Görtler parameter increases with the

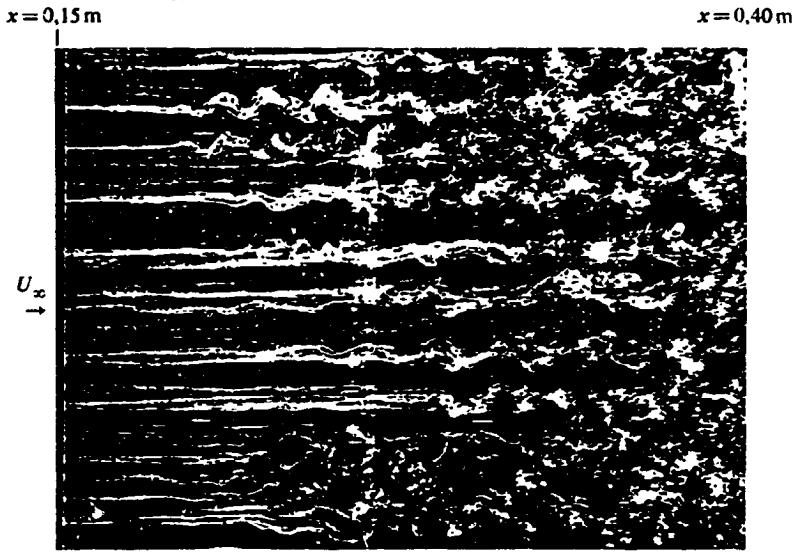

Fig. 30. Development of instabilities with a screen used to produce disturbances. R = 0.5 m; U_∞ = 0.52 m/s; G = 8.3 (in the transition region); x_S = 0.15 m; $y_S/\delta \simeq 0.4$.

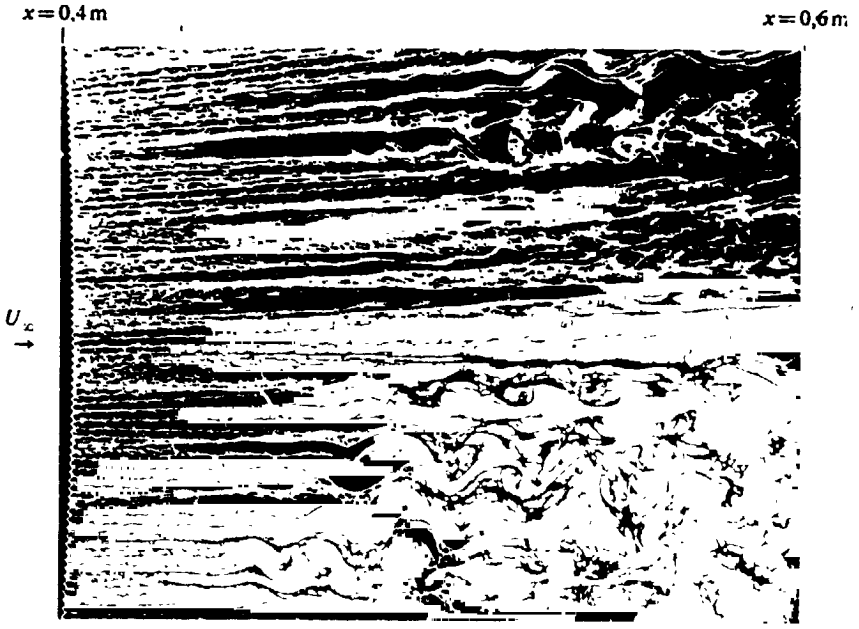

Fig. 31. Development of instabilities with a screen used to produce disturbances. R = 1 m; U_∞ = 0.25 m/s; G = 8.2 (in the transition region); x_S = 0.4 m; $y_S/\delta \simeq 0.4$.

boundary layer thickness or with the run length, it can be stated here -- similar to as in Liepmann [7], [8] -- that the Görtler parameter, as found in the linearized theory, is capable of describing the stability condition of the boundary layer on a concave wall. Liepmann had deduced this on the basis of his experimental findings, according to which the boundary layer always makes a transition at a certain wall curvature ($R = 0.75$ m) independently of U_∞ when a parameter value of $G = 9$ is reached.

Finally, it can be gathered from Figs. 30 and 31 that the longitudinal vortices are actually predominant for the two strongly curved models and that two-dimensional Tollmien-Schlichting waves, in agreement with the linearized theory, do not occur (on this point also see section 2.3 and Fig. 3). As to the question of whether perhaps three-dimensional Tollmien-Schlichting waves are not involved in the transition, this must be discussed in detail later on. Here once again it should just be made clear how important it is to use strongly curved surfaces if one wants to study the development of Gortler vortices and their effect on the laminar-turbuelen transition. Based on this understanding, the strongly curved models with radii of $R = 0.5$ m and $R = 1$ m were used for all further experiments even though, for the reason mentioned above, with these models the development of instabilities can be observed only along a short distance. /151

5.3 The Wavelength of the Longitudinal Vortex Disturbance

According to the linearized theory, the possible longitudinal vortices in the unstable concave boundary layer can assume all wavelengths within a certain region which is covered by the neutral curve (see stability diagram Fig. 2, p. 3). In order to find out which of these finally prevail experiments were again conducted with a screen towed in front of the model. In so doing it turned out, as already discussed in section 5.1.2, that longitudinal vortex components of a certain wavelength are excited in the unstable laminar boundary layer flow which is superimposed by an isotropic disturbance field. As the experiments showed (Fig. 32 a, b, c and Table 2), λ in this situation is a function both of the oncoming flow velocity and the curvature of the model. /152

If with the mean values determined for λ from Fig. 32 a, b, and c one forms the dimensionless parameter

$$K = \frac{U_\infty \lambda}{\nu} \sqrt{\frac{\lambda}{R}} = 195,$$

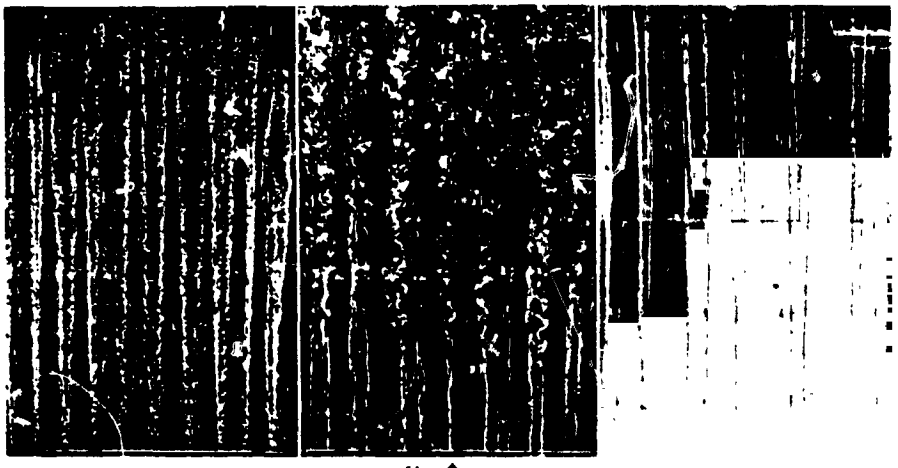

Fig. 32. Development on instabilities using a screen to produce disturbances.

Table 2

point no.	U_∞ [m/s]	R [m]	$\lambda \cdot 10^{-2}$ [m]	K	G
1	0,075	0,5	1,5	195	4
2	0,30	0,5	0,65	212	5
3	0,075	1	2,0	210	3,5

valid for the test conditions in each case, then one obtains almost the same values for all of the experiments listed in Table 2. In the stability diagram they establish K = constant lines which run through the neutral curve and the curves of constant excitation in the vicinity of their minimums, i.e. where the longitudinal vortices of the relevant wavelength are first or most strongly excited.

To be sure, such a finding was to be expected, but the fact that it actually occurred then indicates also in this case the validity of the linearized theory. The deviation in K values can be attributed to the irregularities still present in the flow field. These can also be seen in Fig. 32 a, b and c. They will certainly make themselves very strongly felt because the minimums of the excitation curves in the stability diagram are very flat.

Further experiments with screens of different mesh sizes and mesh shapes showed no effect on the disturbances. To be sure, however, dirt particles which have been caught in the screens can cause deviations from an isotropic distribution of disturbances and thereby of course also cause certain irregularities in the flow field. With the stability parameters

G given in Table 2, together with the corresponding K values, it is possible to specify the flow conditions shown in the photographs in Fig. 32 in the stability diagram. These are labelled 1, 2 and 3 in Fig. 37 (p. 47).

5.4 The Neutral Curve

Initial attempts to establish the neutral curve for the boundary layer on a concave wall have already been made by Wortmann [13]. On a slightly curved model (R = 20 m) and using a rhombus-shaped airfoil he produced a sinusoidal disturbance velocity u running in the span direction somewhat like that assumed in the theoretical solution equation of Görtler [1]. By producing a subcritical stability state by cutting off the boundary layer he was able to visualize how the amplitudes of the disturbance components u first of all decrease and then again increase after a certain distance downstream. The flow state corresponding to the place of reversal from damping to excitation was regarded as the point of the neutral curve. It is marked in the stability diagram by the pertinent ($\alpha\theta$) and G values and lies in the vicinity of the minimum of the neutral curve calculated by Görtler [1] (Fig. 37, p. 47). For several reasons it was decided in the experiments conducted here not to determine other points in the vicinity of the medium. An important factor for this was the circumstance that for this purpose one must introduce very strong disturbances in order to be able to observe or measure them in the non-excited state. Since at the same time the oncoming flow velocity must be selected very small if the flow is to be stable with respect to Görtler vortices along a sufficiently long distance, u and U_∞ can hardly differ from one another by a whole order of magnitude. This is precisely what should be avoided, however, based on what has been said in section 4.3.2. In confirmation of the arguments made there we can here refer to the experience of Wortmann that the location of the neutral point found by him is not independent of the angle of attack of the disturbance airfoil or of the intensity of the initial disturbances. Such a relationship also showed up in the theoretical investigations of Meksyn and Stuart [31] and Grohne [32] using the exmaple of flow between flat parallel walls. /153

Likewise it is difficult to determine points of the neutral curve further to the left of the point of the minimum because this would require the introduction of very wide vortices. As Fig. 33 shows, such vortices are in fact not constant, but rather intermediate vortices are formed of half wavelength. Accordingly, a new flow state exists, which in the stability diagram is shifted to the right with respect to the old flow state into the region of stronger excitation.

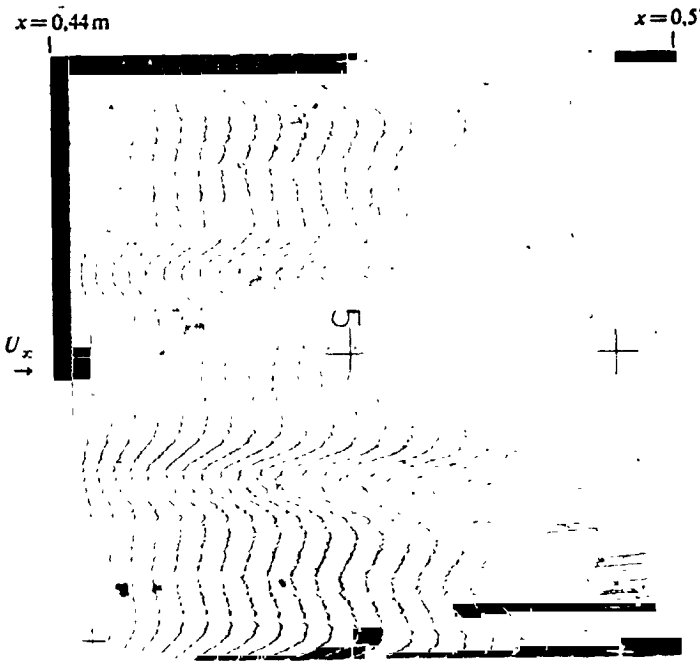

Fig. 33. Disturbances of weakly excited wavelength produced with hot wires together with additional, naturally occurring vortices of half wavelength. R = 1 m; U_∞ = 0.05 m/s; G = 2.86; K = 328; x_S = 0.45 m; $y_S/\delta \approx 0.3$..

Therefore the experiments conducted here to establish the neutral curves were only directed towards determining their sharply rising right branch. To this end, incipient disturbances were produced using the heated wires and at different towing velocities U_∞. These were spaced one after another in the span direction at distances of 0.85, 1.7 and 3.4 cm. To find out whether this would give rise to longitudinal vortices of the intended wavelength excited further downstream, the flow was visualized at three different distances from the leading edge /154
by means of bubble probes at x_S = 0.15, 0.25 and 0.40 m and the flow was photographed. The relevant photographs are joined together in Figs. 34, 35 and 36.[1] The individual series of horizontal pictures show the development stages of the longitudinal vortex disturbance of different wavelengths with the same oncoming flow velocity U_∞ directly behind a bubble probe. Therefore the same stability parameter G is valid for the flow state in the horizontally adjacent photographs. It is given

1. The considerably larger and partially blurred light spots which can be seen in different pictures are air bubbles which have attached themselves to the underside of the model.

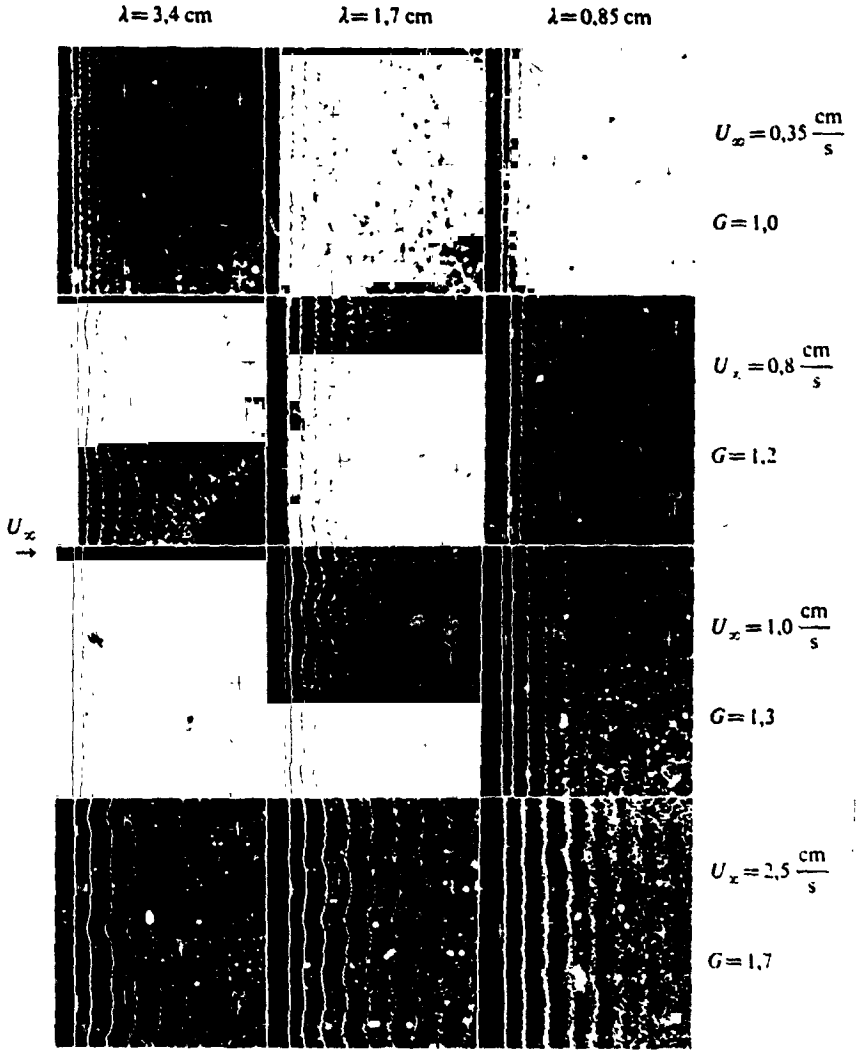

Fig. 34. Longitudinal vortex disturbances of different wavelengths produced by hot wires. Probe location: x_S = 0.15; y_S = 3 mm.

in the right hand margin below the corresponding value of U_∞. The vertically adjacent photographs show disturbances in which initial disturbances of the same wavelength were produced corresponding to the λ values given at the top of each column. The photographs which were taken behind the same probe (at x_S = 0.15, 0.25 or 0.40 m) are grouped together on one sheet in each case.

The flow conditions shown in the individual pictures are given in the stability diagram in Fig. 37. The flow states for the excited vortex disturbances are indicated by circles and by squares for the dampened disturbances. From this it is clear that excited longitudinal vortices only form when a certain

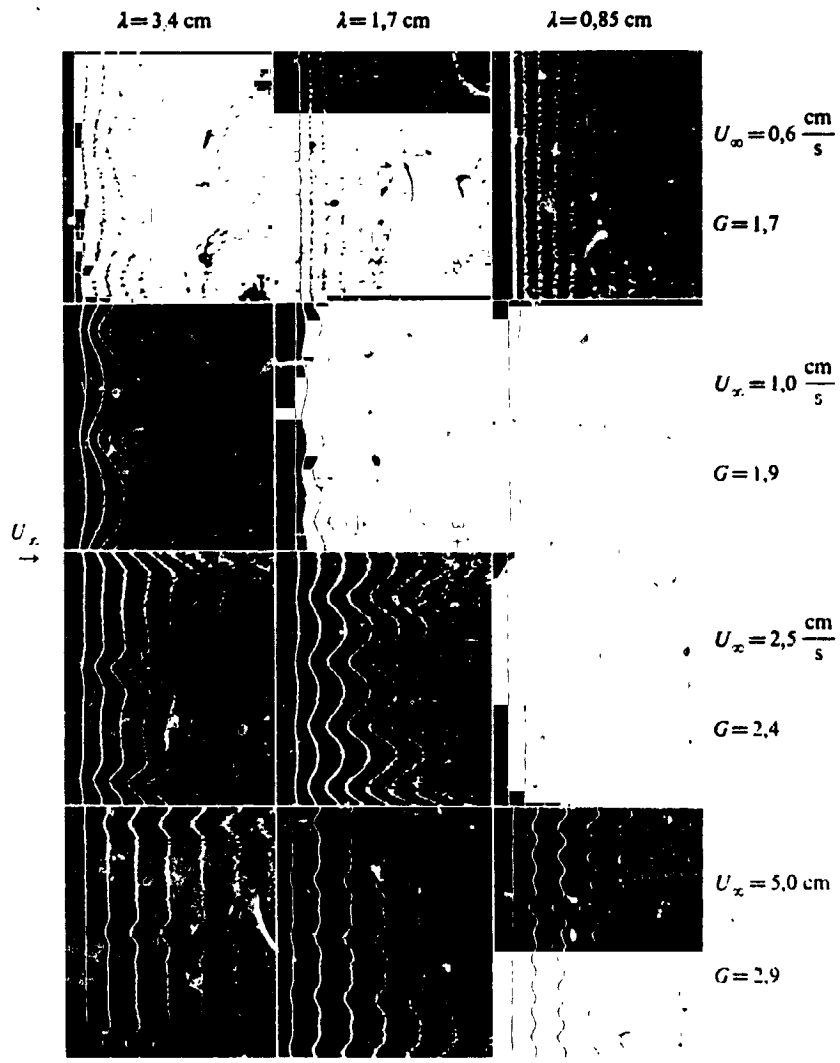

Fig. 35. Longitudinal vortex disturbances of different wavelengths produced by hot wires. Probe location: x_S = 0.25 m; y_S = 4 mm.

parameter value K = f(G) is exceeded. A boundary line (-·-·-) can be drawn between the flow states indicated by the circles and squares. This can be regarded as the portion of the right branch of the neutral curve located in the measuring range. With respect to the curves calculated in [1] or in [2] and [5], it is, to be sure, shifted somewhat to the right. In part, however, this may be due to the fact that the disturbances /157
produced, which lie barely outside the excited region, are damped only imperceptibly, and also in part to the fact that Görtler [1], Smith [2] and Hämmerlin [5] based their calculations of the neutral curve on the Blasius profile determined for the flat boundary layer, whereas according to [33] and [34] the

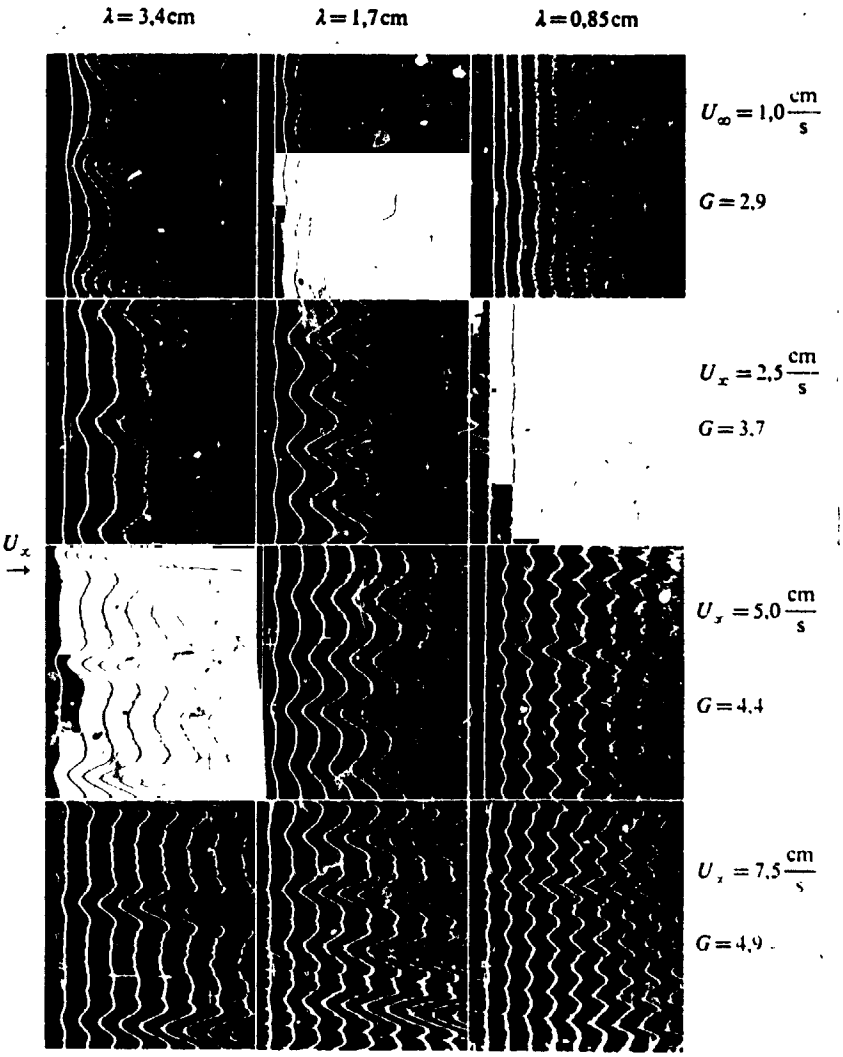

Fig. 36. Longitudinal vortex disturbances of different wavelengths produced by hot wires. Probe location: x_S = 0.4 m; y_S = 5 mm.

boundary layer on a concavely curved wall is somewhat thinner. /158 The experimental evidence for the right branch of the neutral curve here should be regarded as a significant result.

5.5 Excitation of the Longitudinal Vortex Disturbance

In this section we will first of all show purely qualitatively the relationship between excitation and the wavelength of the vortex disturbance. Then for the most unstable magnitude of disturbance the exictation will be determined quantitatively using the measuring method described in section 4.2.

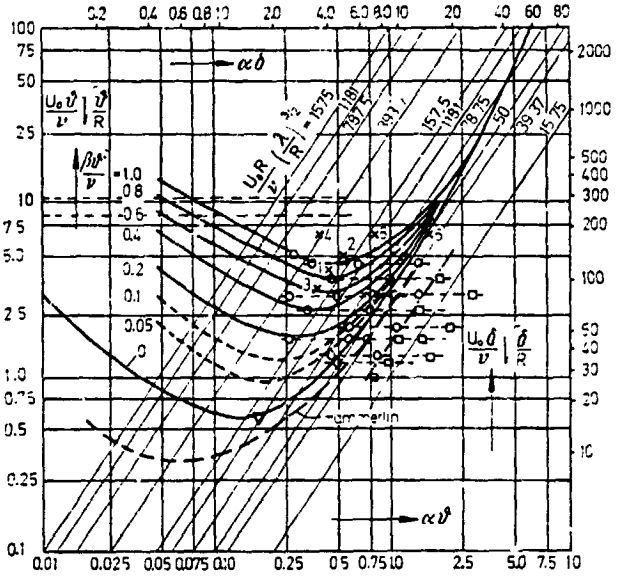

Fig. 37. The stability diagram (from [1], Fig. 8) with the values for the neutral curve obtained by Wortmann and those obtained by the author. ∘ flow state with excited disturbances; ∘ flow state with damped disturbances; -·-·- measured points of the neutral curve; ▽ Wortmann [13]; x additional test points (section 5.3 and section 5.5.1).

5.5.1 The Relationship between Excitation and Wavelength

As already mentioned several times, the curves of constant excitation have pronounced minimums in the stability diagram and that is why for the same stability parameter (G = constant) the longitudinal vortices of different wavelengths are excited to different degrees. This can be simply checked experimentally by introducing longitudinal vortices of different wavelengths but the same initial intensity in the unstable boundary layer at the same oncoming flow velocity U and comparing the degree of their excitation at the same point x. In this case the points /159 P (G;αθ) indicating the flow state in the stability diagram lie along a horizontal straight line which intersects various curves of constant excitation. Consequently, suitable flow photographs at the same place downstream must show longitudinal vortices excited to different degrees.

To what extent this theoretical statement can be confirmed by experiment can be seen from the photographs in Fig. 38. They show the boundary layer flow on the same wall segment. In each case the oncoming flow velocity was U_∞ = 0.06 m/s; the wavelength λ of the longitudinal vortices was successively 3.4, 1.7 and 0.85 0.85 cm. The disturbances were initiated by hot wires with exactly the same initial intensity. The corresponding flow states are indicated in the stability diagram (Fig. 37) by points 4, 5 and 6. Accordingly, point 5 lies in the region of greatest excitation. The pertinent flow photograph is the middle one in Fig. 38. Comparison with the two adjacent photographs immediately shows that here the vortex disturbance is indeed excited to the greatest degree.

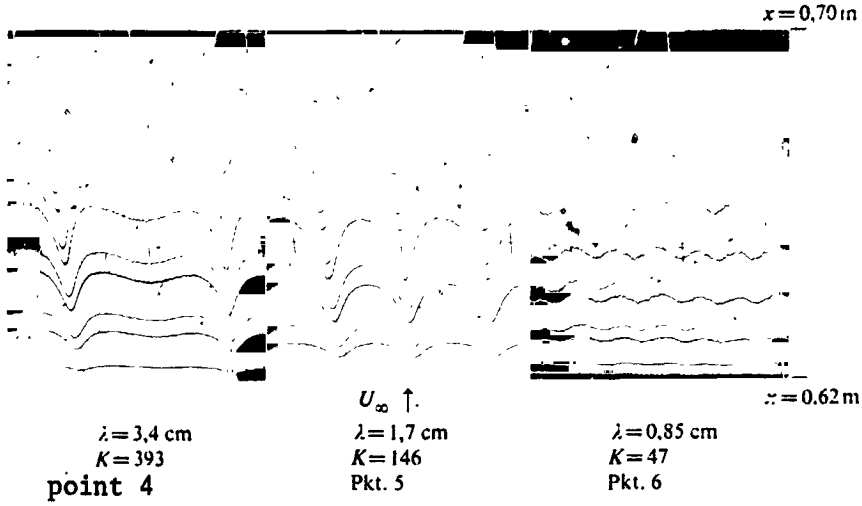

Fig. 38. Excited longitudinal vortices at various wavelengths λ and with the same oncoming flow velocity U_∞ (double exposed photographs). R = 1 m; U = 0.06 m/s; G_S = 6.3; x_S = 0.625 m; $y_S/\delta \approx 0.25$.

5.2.2 Quantitative Determination of the Excitation of the Longitudinal Vortex Disburbance

In order to determine the excitation of the longitudinal vortex disturbance, double exposed timeline photographs taken with the photogrammetric stereocamera were analyzed photogrammetrically. In these experiments the bubbles emanated from horizontal probes which were mounted at 25, 35, 45 and 55 cm downstream from the leading edge and whose distance from the wall was varied within the boundary layer. By this means it was possible to determine the velocity field at different points x as a function of the distance from the wall. The measurements were restricted to the x-y planes along which the velocity component in the direction of the oncoming flow reached its minimum or its maximum, i.e. along the longitudinal sections which are labelled 1 and 3 in Figs. 27 and 28. /160

In order to create a homogeneous as possible flow field the disturbances for these experiments were again initiated with the hot-wire coil. The wavelengths λ were chosen in such a way that the vortex disturbance developed in the region of greatest excitation.

5.5.2.1 Velocity Profiles in the Boundary Layer Disturbed by Excited Longitudinal Vortices

In the longitudinal sections 1 and 3 the velocity component is always w = 0. The velocities U, u and v measured

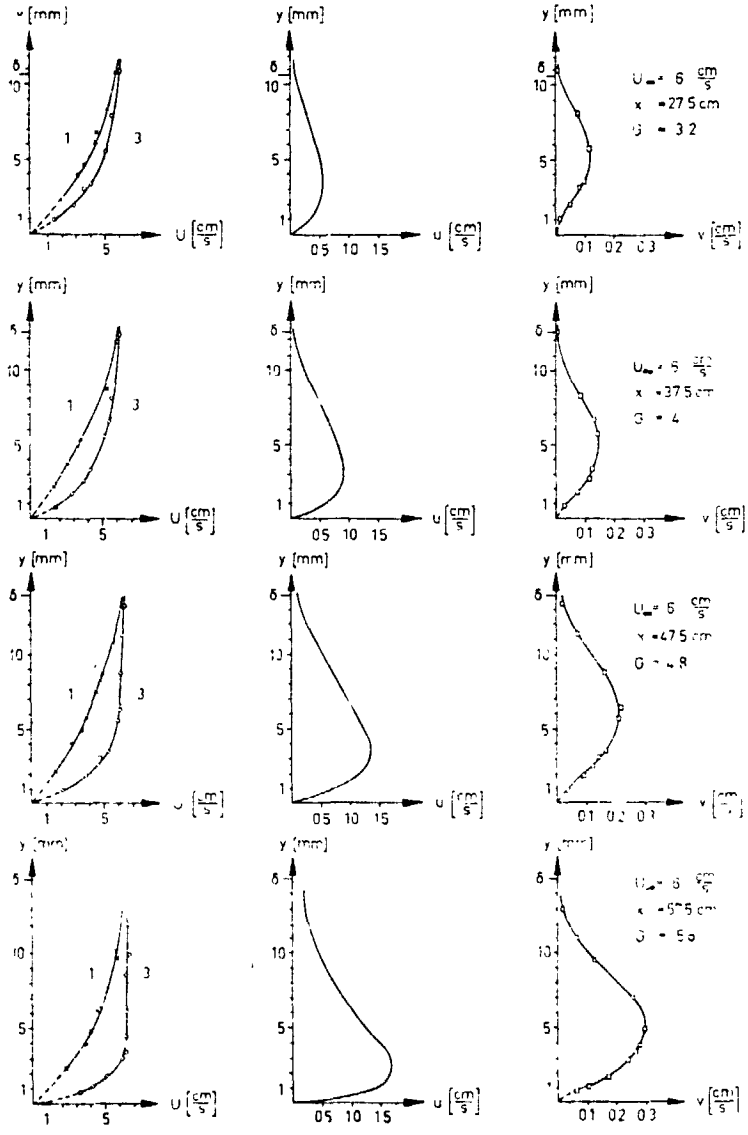

Fig. 39. Profiles of the boundary layer velocity and the disturbance velocity measured in longitudinal sections 1 and 3. U_∞ = 0.06 m/s; R = 1 m; δ = boundary layer thickness at the measuring point.

there at distances of x = 0.275 m, 0.375 m, 0.475 m and 0.575 m behind the leading edge at an oncoming flow velocity of U_∞ = 0.06 m/s are plotted in Fig. 39 over the distance from the wall. This clearly shows how the vortex disturbance develops downstream and how the boundary layer profiles are affected by this. The velocity profiles are affected in such a way that next to the wall the velocity gradients ($\delta U/\delta y$) of the profiles U(y) in

longitudinal section 1 become smaller and smaller in comparison with those in longitudinal section 3. It is therefore obvious when the laminar-turbulent transition is initiated in longitudinal section 1, as will be shown later on.

Here it should be mentioned that the tendency which can be recognized in Fig. 39 of the disturbance components u and v to decrease downstream the distance from the wall of their maximum corresponds in the same way to the linearized theory as the tendency of the disturbances to extend beyond the boundary layer with an increasing degree of excitation.

In Fig. 40 the amplitudes measured at x = 0.457 m for the disturbance velocities are plotted over the distance from the wall y. Here also in order to make another comparison with the theory the eigenfunctions calculated by Hämmerlin [4] corres-

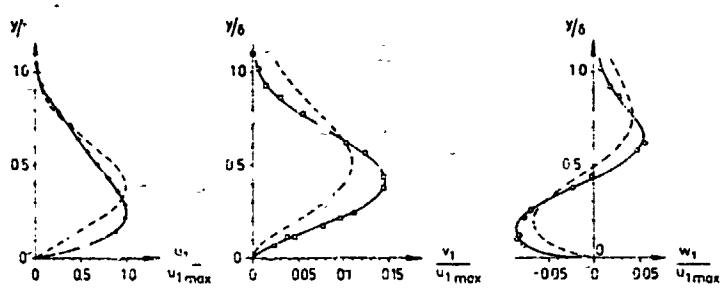

Fig. 40. Amplitude distribution of disturbance velocities. R = 1 m; G = 4.8; U_∞ = 0.06 m/s. ——— Measured curve; ---- Theoretical curve.

ponding to this flow state are also plotted. Accordingly, both curves are in agreement inasmuch as u is greater in each case than v and w and u reaches its maximum at a smaller distance from the wall than v. By contrast, the measured disturbances unlike the calculated ones, extend only insignificantly beyond the boundary layer.

5.5.2.2 The Excitation Curve /162

To make clear to what extent the disturbance motion is excited downstream, Fig. 41 shows the maximum disturbance velocity u_{max} measured at different points downstream with respect to the value found at x = 0.275 m plotted over x and G. In addition, the ratio u_{max}/U_∞ is also given for each measuring point so that the development of the absolute values of u_{max} with respect to U_∞ can be followed. Similar to what was found by Tani [12], the excitation does not diminish with an increasing Görtler parameter. The slope of the curve here, however, is is somewhat steeper than that found in Tani.

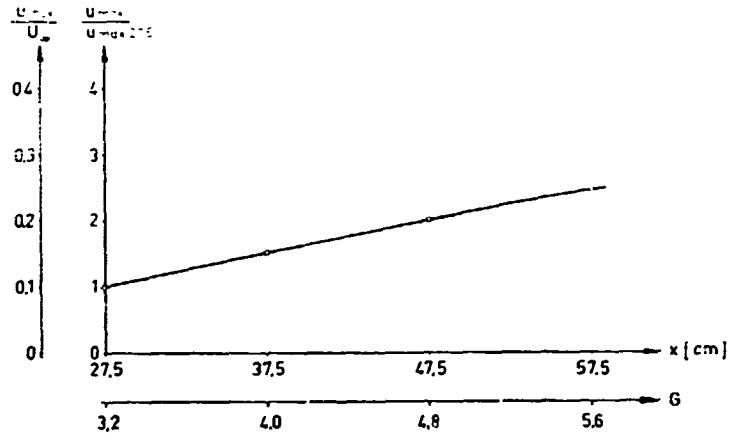

Fig. 41. Curve of excitation with increasing distance from the leading edge. U_∞ = 0.06 m/s; R = 1 m.

5.6 The Laminar-Turbulent Transition /163

As already described in section 2.3, one aim of these experiments was to especially emphasize the effect of longitudinal vortex disturbance on the laminar-turbulent transition. Therefore, in contrast to Tani [12], Aihara [10], Tani and Aihara [15] and Wortmann [13], [14], the curvature of the model surface was chosen so large that the boundary layer is as stable as possible with respect to Tollmien-Schlichting waves up to the transition. For this same reason, neither were any periodic disturbances produced in the boundary layer, for example by means of a transversely oscillating band (Tani and Aihara [15]) or by means of a disturbance airfoil making rotary oscillations. This means, of course, that possible periodic, nonsteady events may nevertheless result and have an uncontrolled effect thus considerably complicating a systematic study precisely in the transition zone. Therefore we did not so much pursue the objective of giving a generally valid description of the transition process as rather we tried to represent the events in the existing flow field as clearly as possible and compare them with existing findings.

In contrast to the periodic disturbances, the longitudinal vortices in all of the experiments which are described in this section were initiated with hot wires. Thus an extremely regular flow field always exists up into the transition zone.

5.6.1 The Longitudinal Vortex Field

If above the boundary layer in question was said to be stable with respect to Tollmien-Schlichting waves, what was means by this was stable in the sense of the linearized theory

for the case of R = 0. If, however, a two-dimensional laminar boundary layer is superimposed with counterrotating longitudinal vortex pairs, then it becomes deformed three-dimensionally and velocity profiles of greater and lesser stability are formed (see Fig. 39). The profiles in longitudinal sections 1 become especially unstable where the disturbance component is directed against the direction of the main flow. As a result, the Tollmien-Schlichting stability limit can be reached sooner here than is predicted by the theory for the Blasius boundary layer. As will be shown later on, the transition process actually begins in these zones.

Up until then, however, the longitudinal vortex field is stable. A secondary instability, indicated by the appearance of twisted interfaces between the longitudinal vortices as described by Wortmann [14], could not reproducibly be presented here. In particular, we did not succeed in finding by means of measurements the associated steady velocity profiles with two points of inflection (cf. Fig. 39). The attempt to visualize them as did Wortmann [14] using a vertical probe ran into considerable difficulties, since the bubble lines which emanate from a probe wire perpendicular to the surface are bent in the z direction as a result of the rotational motion of the longitudinal vortices (Fig. 42). As a result the individual bubbles get into longitudinal sections with different velocity distributions U(y). If, as happens in the photographing process, one examines the timelines forming in this way in a projection on the longitudinal section in which the probe wire is located, then indeed one also sees curves with two points of inflection (Fig. 43 b and c), but accordingly these do not represent velocity profiles in the x-y plane. These are obtained in the boundary layer flow only for the special case in which the bubble probe is located exactly in a longitudinal section 1 (Fig. 43 a) or 3 which at the same time falls in an x-y plane. Both conditions could be met only rarely and at random in these experiments, since the longitudinal vortex field easily moved back and forth in the span direction of the specified vortex with λ does not stand in a certain ratio, which is not entirely clarified in the experiment in question, to the boundary layer thickness. Of course, with the boundary layer increasing in the flow direction such a ratio can only be maintained only at indi-

/164

/165

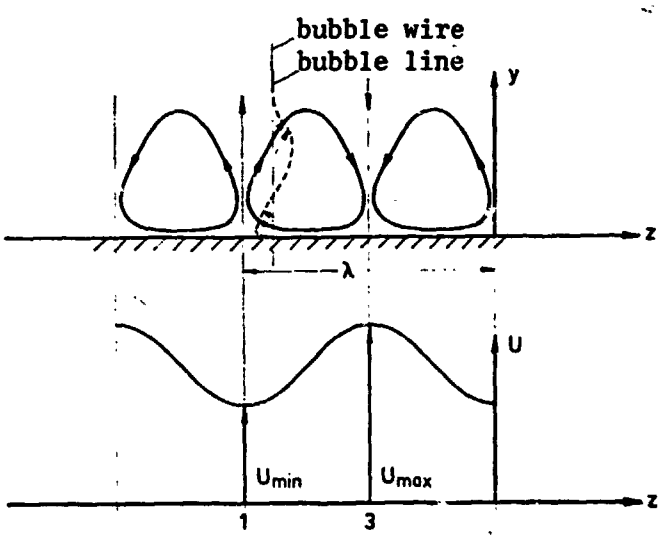

Fig. 42. Release of hydrogen bubbles from a vertical probe in a boundary layer flow disturbed by longitudinal vortices.

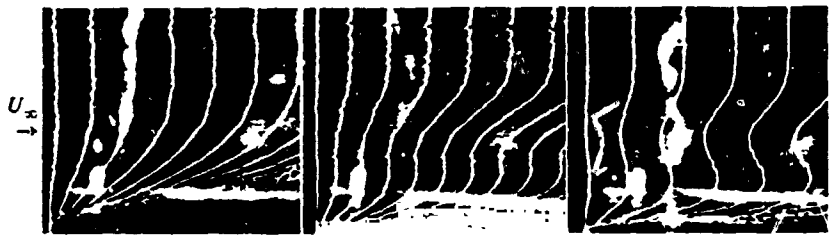

Fig. 43. Bubblelines behind a vertical prove (a) in longitudinal section 1; (b) and (c) between longitudinal sections 1 and 3. R = 1 m; x_S = 0.45 m.

vidual points. Based on this view, it was decided not to visualize velocity profiles in a systematic sequence for different stability states. Quantitative data in this regard was obtained exclusively by photogrammetric analysis of stereophotographs, by means of which the three-dimensional distortions of the timelines are taken into consideration.

5.6.2 Secondary Instability

If the velocity profiles superimposed by the excited longitudinal vortex disturbance of the laminar boundary layer in longitudinal section 1 have reached a certain degree of instability, then a new disturbance is created there. Therefore in what follows it will be referred to as a "secondary instability." In timeline photographs with the line of sight on the surface of the model this first manifests itself through a local concentration of timelines limited to longitudinal section 1 (Fig. 44, detail "A"). The latter is equivalent to a decrease in velocity or stagnation. As a result, a thickening of the boundary layer occurs and an increase in the distance between the axes for the pair of longitudinal vortices in question. The following fluid, which arrives undelayed, runs into the stagnated fluid and tries to flow past it. This increases the spanwise vorticity. Immediately behind the stagnation point the flow appears rather accelerated according to the spaces between the timelines, in the process of which the axes of the longitudinal vortices again approach each other (Fig. 44, detail "B").

This process repeats itself in a periodic manner. The letters "C" and "D" in Fig. 44 mark the stagnation points which precede that described at "A." In contrast to point "A", points "C" and "D" are already in a more excited state. In this connection, especially in stereoscopic examination, the rolling

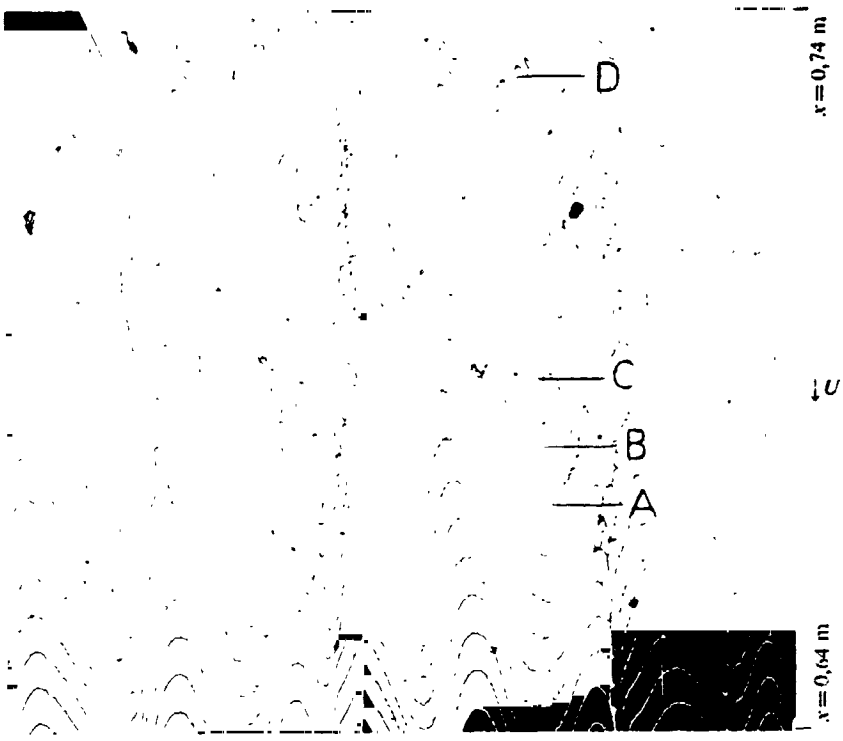

Fig. 44. Creation of the secondary instability. R = 1 m; U_∞ = 0.075 m/s; K = 168; G = 6.5 (at the point of the secondary instability at "A"; x_S = 0.6 m; $y_S/\delta \approx 0.3$.

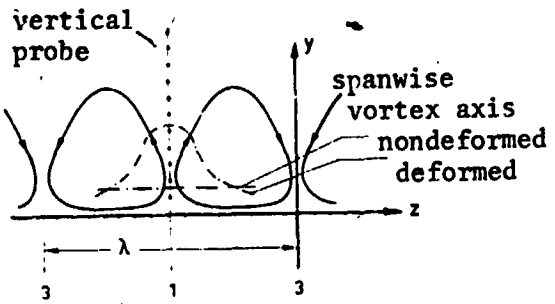

Fig. 45. Deformation of the spanwise vortex axes in the longitudinal vortex field

process, or the increase in spanwise vorticity, stands out more and more clearly. At the same time, the spanwise vortex axis, which at first runs in the z direction, is bent upward in the manner sketched in Fig. 45 by the superimposed longitudinal vortex so that the spanwise vortex at "D" in Fig. 44 already seems to be divided into a left half and a right half. /166

The rolling process, or the development of a spanwise vorticity concentration, is represented somewhat more clearly in the side view (projection on an x-y plane) if the timelines are produced at a vertical probe and if this is located approximately in a longitudinal section 1. In this case the stagantion can first be recognized by a thickening of the boundary layer going out from the wall (Fig. 46, detail "A"). A zone of increased shear due to the sharp difference in velocity /167

Fig. 46. Creation of the secondary instability in the x-y plane. R = 1 m; U_∞ = 0.18 m/s; K = 141; x_s = 0.4 m; G = 7.4 (at the point of the pronounced spanwise vortex at "D", x = 0.575 m).

is formed between the staganted fluid and the undisturbed outer flow. This in indicated in Fig. 46 by the compression of the timelines. The stagantion points preceding one another again turn out to be in a more excited state in each case. In the far right of the photograph in Fig. 46 a pronounced spanwise vortex has already formed itself at detail "D".

Similar hydrogen bubble pictures using the same photography arrangement were obtained for the laminar-turbulent transition of a flat boundary layer by J. Nutant [35] and F. H. Hama and J. Nutant [36]. In this connection, however, they did not speak of stagnations, but rather they explained the occurrence of such forms by the rising up of Tollmien-Schlichting wave fronts from the surface. This explanation cannot be accepted here, since no indications of any kind of Tollmien-Schlichting waves are to be seen up to the appearance of the secondary instability, nor can they be detected with hot-wire anemometers. It is equally impossible to apply the interpretation of similar instability phenomena, vusualized by Meyer and Kline [37] using a colored liquid in a flat boundary layer, to the instability phenomena found in these experiments. Those authors spok of "lifted-up low-speed streaks," which of course also express themselves in the form of a thickening of the boundary layer, but below these the liquid moves at an accelerated rate, a fact which is stressed at the same time. Here, on the other hand, stagnations are involved which emanate from the surface /168
of the wall in the oncoming flow and which only increase in the y-direction in the course of their excitation (from left to right in Fig. 46).

Of the numerous articles on hot-wire studies which have been conducted in flat and also in concave boundary layers, only those by L. S. G. Kovasznay, H. Komoda and B. R. Vasudeva [38] give indications of an instability form of this kind. In this con-

nection, the above authors speak of "slow moving bumps" which, like in these experiments, move under layers of high stress. In [38] in agreement with the theoretical statements in this regard by J.T. Stuart [30] special attention is drawn to the latter phenomenon and also to its action during the laminar-turbulent transition. In these articles little is said about the cause which leads to the stagnations, the "lifted-up low-speed streaks" or the "slow moving bumps." The author of this article suspects local separation of flow as soon as the velocity profiles in longitudinal sections 1 -- the zones of low velocity -- have formed a point of inflection on the wall due to the superimposed longitudinal vortices (cf. Fig. 43 a, p. 53). In order to give a definitive explanation of this it is intended in later experiments to make measurements of the velocity gradie gradients on the wall with hot film flush with the surface.

Finally, in order to be able to say something about the dependence on time of the laminar boundary layer flow disturbed by primary and secondary instabilities, a few specific hot-wire measurements were made in the zones of larger and smaller velocity. To this end, two hot-wire probes were used. These were located at the same (x,y) point but were moved with respect to one another in the z-direction. In order to know or check their position in the easily fluctuating longitudinal vortex field during the measurement interval the flow was visualized at the same time. Fig. 47 shows a corresponding photograph. The bubbles were generated continuously on a horizontal cathode wire. The primary instability, i.e. the longitudinal vortices, can, as before, be recognized by the zones running in the longitudinal direction of larger bubble density (longitudinal section 1) and smaller bubble density (longitudinal section 3) (cf. Fig. 21, p. 33), and the secondary instability, viewed in the x-direction, can be recognized by the intermittent local bubble concentrations (detail "A"). In the picture it is quite clear that these are strictly limited to the longitudinal section 1. Of the two hot-wire probes one in each case is located in a longitudinal section 1 and a longitudinal section 3.

The result of the hot-wire measurement can be seen from the oscillogram in Fig. 48. The traces shown there were produced by an AC measurement. This particularly emphasizes the fluctuations in velocity over time which are reflected by the vertical deflection. The horizontal deflection represents the time axis. Since the time interval of the measurement also includes the point in time of the photograph it is possible to coordinate the measured velocity curve with the corresponding location in the velocity field. This result of the measurement confirms what can be seen on the basis of purely visual evidence (Fig. 47), namely that no fluctuations of velocity of any kind occur in longitudinal section 3 (upper line in Fig. 48). In longitudinal section 1, on the other hand, where secondary

/170

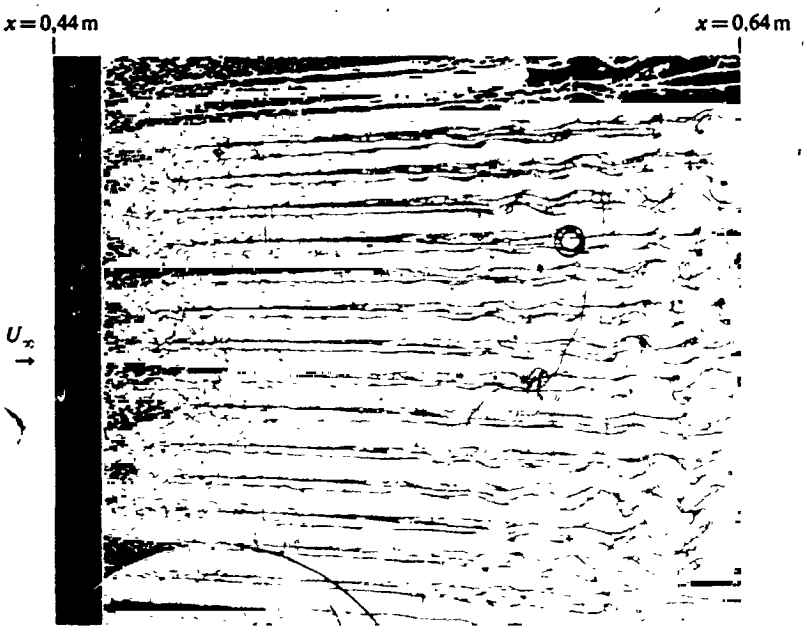

Fig. 47. Laminar boundary layer flow disturbed by primary and secondary instabilities, visuzlized by the continuous generation of bubbles on a horizontal cathode wire. The hot-wire probes which are also photographed are located in a longitudinal section 1 (upper probe) and a longitudinal section 3 (lower probe). R = 1 m; U_∞ = 0.25 m/s; K = 196; G = 8.5 (at the point of the hot-wire probes); $x_{\text{hot-wire probe}}$ = 0.58 m; $y_{\text{hot-wire probe}}/\delta \approx 0.2$.

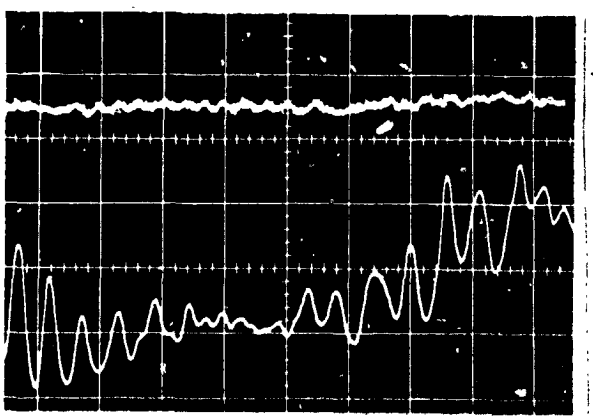

Fig. 48. Oscillogram of the hot-wire measurement (AC measurement). For the vertical deflection one unit of grid spacing = 0.065 m/s and for the horizontal deflection one unit of grid spacing = 0.1 s. The measurement in longitudinal section 3 is represented by the upper trace and the measurement in longitudinal section 1 by the lower trace.

instabilities can be visualized, periodic velocity fluctuations occur between 0-0.3 U_∞. The large irregularity of the amplitude distribution is due to the twisting motion of the longitudinal vortex field. This can already be seen in Fig. 47 and is described in more detail in the next section. What this causes is that the fixed hot-wire probe lies exactly in longitudinal section 1 of the longitudinal vortex field only for a brief time. The frequency is about 12.5 Hz and thus lies in the range of the Tollmien-Schlichting waves. In contrast to these, however, the secondary instability found here does not involve a two-dimensional wave motion nor a three-dimensionally deformed two-dimensional wave motion, but rather a disturbance motion which, viewed in the z-direction, is limited to the longitudinal zones of small velocity U in the longitudinal vortex field.

So called spikes, like those, for example, pointed out by P.G. Klebanoff, K.D. Tidstrom and L.M. Sargent [39] and L.S.G. Kovaszny, H. Komaoda and B.R. Vasudeva [30] in the oscillograms of their hot-wire measurements and which, according to the last named authors, are necessarily connected with the appearance of a kink in the zone of increased shear, have so far not been found. This is in agreement with the statements of I. Tani and Y. Aihara [15] and H. Komoda [40]. This is in spite of the fact that also in the present experiment the zones of increased shear showed a kink at the start of the rolling process (Figs. 46 and 49). However, it has been shown in [15] and [40] that precisely when the boundary layer is very severely deformed three-dimensionally by airfoil-shaped disturbance generators, then no spike are to be found.

Finally, to give an idea of the magnitude of the excitation of a secondary disturbance, or of its development in time on its path downstream, timelines emanating from a vertical probe were photographed with a 16 mm movie camera. This moved with the outer flow at a speed of about 0.8 U_∞ . The photography axis here runs in the z-direction. The result is shown in Fig. 49. The vertically arranged partial pictures there were cut out of a filmstrip. They span time intervals in each case of 0.1 sec. In the uppermost partial picture the secondary instability can already be recognized by the slight increase in thickness of the boundary layer going out from the wall and by the zone of increased shear forming above this. Just as both of these features become more and more pronounced, the spanwise vorticity also increases. This is first of all reflected by a bend in the shear layer. The latter is comparable to the kink described by Kovasznay, Komoda and Vasudeva [38]. Whereas in this experiment, however, a rolling process can be observed in the course of further excitation up to the formation of a discrete spanwise vortex, noting of this sort was described in [38]. /171 /172

In summary ti can be stated that the seconday instability originates in longitudinal section 1 where the longitudinal

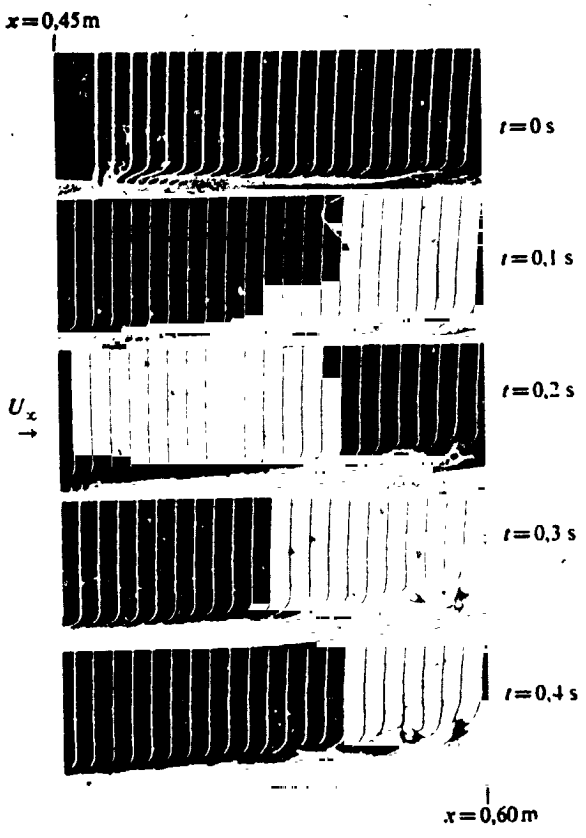

Fig. 49. Excitation over time of an individual secondary instability on its path downstream up to the formation of a pronounced spanwise vortex. Photographed by a camera travelling with the model. R = 1 m; U_∞ = 0.18 m/s; K = 141; x_S = 0.45 m; $y_S/\delta \approx 0.25$; G_S = 6.1; camera velocity = $0.8 \cdot U_\infty$. (Even at the greatest possible picture-taking rate of 64 frames per second with the Bolex camera used a certain amount of movement blur could not be avoided. As a result, especially the bubbles present in lower density in the vicinity of the wall are lost.)

vortex component u is directed against the primary flow velocity. It forms when the velocity profiles become steeper and steeper as a result of the superimposed excited longitudinal vortex disturbance (Fig. 39) and, as suspected by the author, it finally acquires a point of inflection (Fig. 43 a, p. 53). At first, periodic velocity slowdowns occur which emanate from the wall and result in stagnation points in the fluid (Figs. 44, 46 and 49). At the same time, regions of increased shear or spanwise vorticity concentrations are created above the stagantion points. These are caused by the difference in velocity between the slowed down fluid and the fluid flowing above it which is not slowed down. This disturbance motion which characterizes the secondary instability is excited downstream (Fig. 49) until the picture of a pronounced transverse vortex shows up in a vertical section (x-y plane) through its center. The frequency of the fluctuations in velocity acting as stagantion points was determined to be about 12.5 Hz at amplitudes up to $0.3\ U_\infty$.

5.6.3 Sinuous Motion of the Longitudinal Vortex Streets

In the boundary layer flow disturbed by primary and secondary instabilities a serpentining of the longitudinal vortex streets can often be observed (Fig. 50). Such a phenomenon is already familiar from photographs of boundary layer flows which have been disturbed by individual roughness elements, from the unstable Couette flow in the gap of a Taylor cylinder and also from boundary layer flows on heated walls (among others, P. Idrac [41]). In this connection, the latter are especially

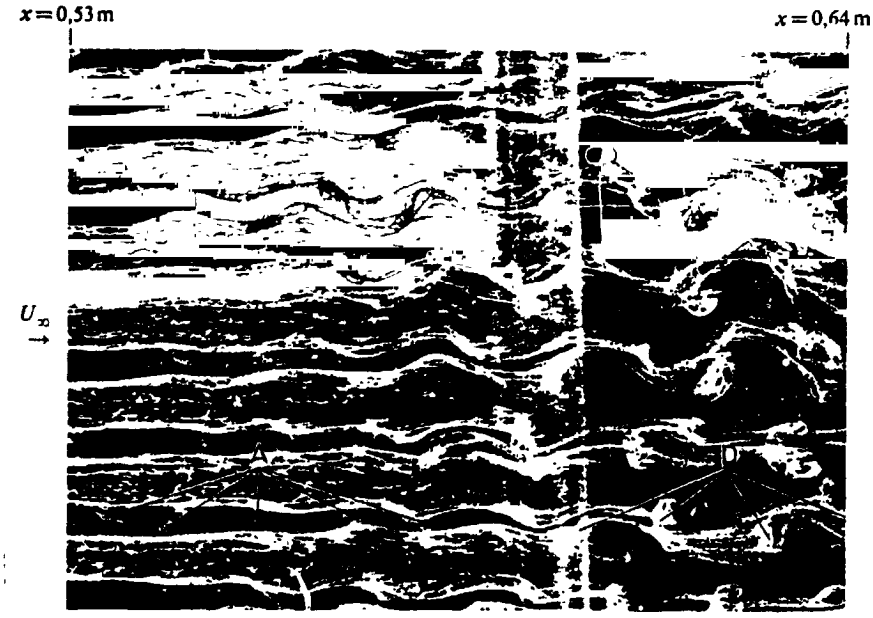

Fig. 50. Boundary layer flow disturbed by primary and secondary instabilities with serpentining longitudinal vortex axes, visualized by continuous bubble generation by a horizontal probe. R = 1 m; U_∞ = 0.25 m/s; K = 196; G = 8.2 (at x = 0.60 m); x_S = 0.45 m; $y_S/\delta \approx 0.2$.

interesting, since according to H. Görtler [42] and K. Kirchgässner [43] a direct analogy exists between the possible instabilities on heated walls and on concave walls. With regard to the experiments just on concave walls, the sinuous motion can certainly be perceived in the smoke thread photographs by I. Tani and J. Sakagami [11], but it is not mentioned in the text of the article in question. In addition, Wortmann has discussed another oscillatory motion in [14] which he designates as an instability of the third order. It was excited artificially by an airfoil making rotary oscillations and about two periods following its creation it resulted in the laminar-turbulent transition.

In the experiment under discussion it was not possible to directly visualize how the laminar-turbulent transition is brought about by the sinuous motion (Figs. 30 and 52). Nevertheless, the question must remain unanswered of whether in this case an instability of the third order is really involved or merely a secondary phenomenon of the secondary instability. The latter possibility seems to be indicated by the fact that the serpentining is often, but not necessarily, linked with the formation of the spanwise vortex. Even in an instantaneous flow photograph, like that shown in Fig. 50, straight longitudinal

/173

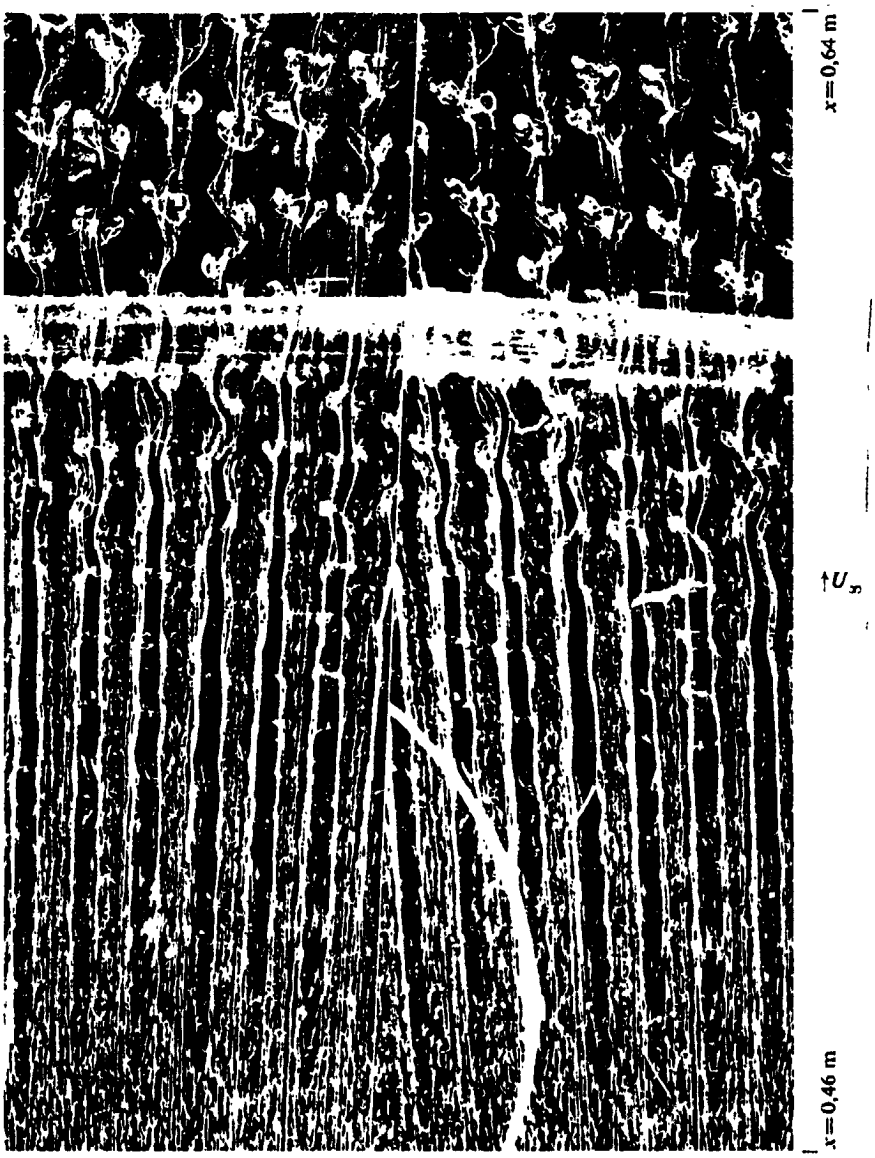

Fig. 51. Stereophotograph of a laminary boundary layer flow disturbed by primary and secondary instabilities. R = 1 m; U_∞ = 0.28 m/s; K = 218; G = 8.4 (top half of picture); x_S = 0.45 m; $y_S/\delta \approx 0.2$.

vortex streets can also be seen along with undulating streets. The same is true for the pictures made by I. Tani and J. Sakagami [11] and for the pictures made in the visualization experiments on heated walls. A regular sinuous motion can be found only with the Taylor cyliners where the flow can flow only laterally past the possibly occurring stagnation points. The serpentining is missing almost completely in the photograph shown in Fig. 51. The reason for this may be that in this case

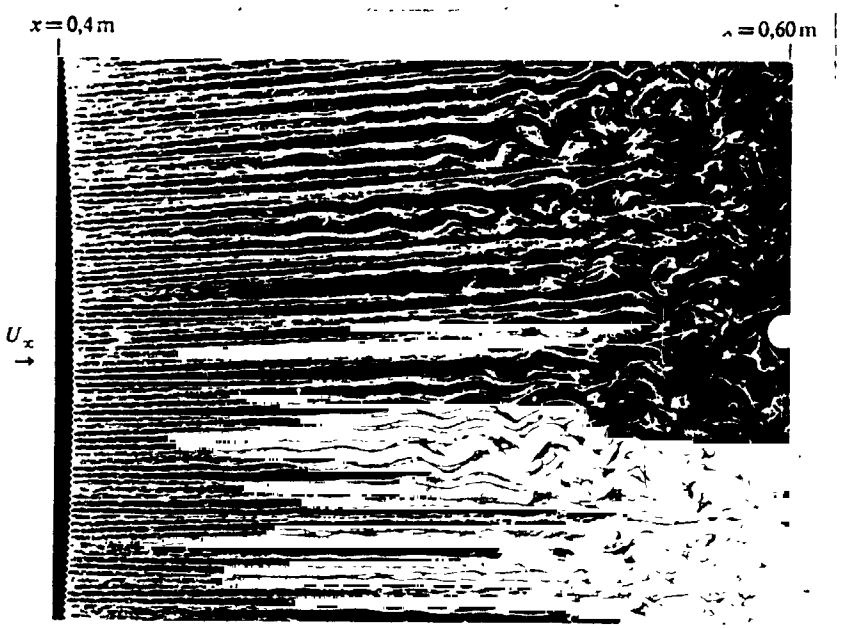

Fig. 52. Laminar-turbulent transition brought about by the sinuous motion of the longitudinal vortex axes. R = 1 m; U_∞ = 0.30 m/s; K = 230; G = 8.5 (in the transition zone); x_S = 0.4 m; $y_S/\delta \approx 0.2$.

the wavelength stands in a particularly favorable ratio to the boundary layer thickness. Under these conditions, an especially regular flow field is in fact also always formed. If this does not happen, i.e. if somewhere the flow preferably goes around the stagnation points on one side, then this initiates a serpentine motion. However, if such a motion is once excited, then it intensifies downstream until the lateral deflection of the longitudinal vortex axis has become so sharp that the direction of motion can no longer reverse itself (Figs. 30 and 52). From this point on the ordered bubble structures vanish entirely and the boundary layer becomes turbulent. /175

Finally, to clarify whether the sinuous motion is a necessarily forming instability of the third order or a necessary step in the laminar-turbulent transition, it will be attempted in later experiments to stabilize the longitudinal vortex fields so that serpenting of the vortex axes is prevented as much as possible. In this way it would be possible to determine whether also the secondary instability with further excitation is capable of producing the laminar-turbulent transition.

6. Summary

In order to round out the experimental studies conducted in the past on concave walls a special effort was made in these experiments to discover the direct effect of a longitudinal vortex disturbance on the laminary-turbulent transition. It was therefore necessary to try to avoid as far as possible other disturbances such as Tollmien-Schlichting waves. We succeeded in this to a large degree by selecting walls of especially severe curvature (R = 0.5 m and R = 1 m). In the boundary layer of these walls the instability caused by the centrifugal force is so strong that at small velocities the laminar flow already becomes unstable with respect to counter rotating longitudinal vortex pairs and the turbulent transition occurs before it becomes unstable with respect to Tollmien-Schlichting waves according to the linearized theory.

In carrying out the experiments the disturbances were first visualized using the hydrogen bubble method. These disturbances develop naturally in the unstable boundary layer. They have a three-dimensional character and exhibit the periodicity in the span direction assumed in the theory. The same result turned up when the oncoming flow was superimposed by any incipient disturbances in an isotropic distrubution produced by a screen in front of the model. The greater regularity of the flow field obtained by this arrangement made it possible to determined the wavelength of the longitudinal vortes disturbance under the experimental conditions in each case. In addition, it was also possible to establish a relationship, explained by the linearized theory, between the wavelength and the oncoming flow velocity and the curvature of the model.

By introducing a new disturbance generator in the form of hot wires we created, on the one hand, a reproducible flow field suitable for measurements and, on the other hand, we now succeeded in producing incipient disturbnaces which were small enough so that we could carry our further comparisons between experiments and the linear theory. These comparisons concern the form of the three-dimensional instability, the effect of the magnitude of the wall curvature, the right branch of the neutral curve, the dependency of excitation on wavelength and the development of the excitation downstream.

Stereophotographs were produced in order to determine the boundary layer phenomena in three dimensions. Photogrammetric analysis of these photographs made it possible to determine the magnitude and direction of the velocity in the flow visualized by hydrogen bubbles. Thus it was possible for the first time to completely represent the three-dimensional development of the disturbances. The difficulty of producing a total picture of the flow field from point-determined test values was avoided.

In the course of the non-linear development of the longitudinal vortex disturbance a secondary instability was observed. /177
It arises where the u component of the primary disturbance is directed against the oncoming flow and it makes the boundary layer profile unstable. Like the Tollmien-Shclichting waves, it possesses a periodicity in time, but it differs from Tollmien-Schlichting waves in terms of its three-dimensional character. Using hot-wire measurements with simultaneous visualization we succeeded in showing that the secondary flows are strictly limited to the longitudinal zones of smaller velocity U. They can first be detected by a stagnation emanating from the surface. Spanwise vorticity concentrations then form above the stagantion points due to the difference in velocity between the slowed down and non-slowed down particles of fluid. These spanwise vorticity concentrations are first of all reflected as zones of increased shear and later, in the course of their excitation, they trigger a rolling process. The latter results in a bend in the shear layer and ultimately leads to pronounced spanwise vortex structures.

So for it has not been possible to determine the direct effect of the secondary instability on the laminar-turbulent transition, since the transition is triggered prematurely by a new additional disturbance motion. This always turns up where the flow around a stagnation point is not symmetrical but rather predominates on one side. This causes a lateral deflection of the corresponding longitudinal vortex axis and specifically excites a sinuous motion of the same which grows continually stronger downstream until ultimately the vortex streets flutter away and the boundary layer becomes turbulent. In order to determine the direct effect of the secondary instability on the transition it will be attempted in later experiments to stabilize the longitudinal vortex streets using artificial means. In a like manner, a theoretical study of the stability of longitudinal vortex streets with and without secondary disturbances with respect to serpentining could contribute to the further clarification of this problem.

I would sincerely like to thank Prof. H. Görtler for suggesting that I deal with this topic, for his continuous support and for his guiding advice in the carrying out of this study.

I would kindly like to thank Dr. Colak-Antic for his constant willingness to discuss things with me and for many helpful instructions.

I owe a special debt of thanks to A. Maier, Engineer, for developing and repairing the electronic equipment and to G. Kaufhold and K. Mayer for their careful and laborious execution of the mechanical work. I would like to thank /178
Miss. E. Steiert for her careful execution of the extensive photographic and graphic work.

REFERENCES

1. Görtler, H, "Concerning a three-dimensional instability of laminar boundary layers on concave walls," Nachr. Wiss. Ges. Göttingen, Math.-Phys Kl., New Series I, 2, 1-26 (1940).

2. Smith, A.M.O., "On the growth of Taylor-Görtler vortices along highly concave walls," Quart. Appl. Math. 13, 233 (1955).

3. Taylor, G.I., "Stability of a viscous liquid contained between two rotating cylinders," Philos. Trans. Roy. Soc. London Ser. A, 223, 289-293 (1923).

4. Hämmerlin, G., "Concerning the eignevalue problem of the three-dimensional instability of laminar boundary layers on concave walls," J. Rat. Mech. Anal. 4, 271-321 (1955).

5. Hämmerlin, G., "On the theory of three-dimensional instability of laminar boundary layers," Z. Angew. Math. Phys. 7, 156-164 (1956).

6. Clauser, M. and Clauser, F., "The effect of curvature on the transition from laminary to turbulent boundary layer," National Adivsory Committee for Aeronautics Techn. Note No. 613 (1937).

7. Liepmann, H.W., "Investigations on laminar boundary layer stability and transition on curved boundaries," NACA Wartime Report W. 107 (1943).

8. Liepmann, H.W., Investigation of boundary layer transition on concave walls. NACA Wartime Report W87 (1945).

9. Gregory, N. and Walker, W.S., "Tthe effect of transition of isolated surface excrescences in the boundary layer," ARC Repl, R & M No. 2779, 1-10 (1956).

10. Aihara, Y., "Transition in an incompressible boundary layer along a concave wall," Bull. Aeron. Res. Inst., Tokyo Univ., 3, 195 (1962).

11. Tani, I. and Sakagami, J.,"Boundary layer instability of subsonic speeds," Proc. Int. Counc. aeron. Sci. Stockholm, 1962, p. 391 (Spartau (1964).

12. Tani, I., "Production of longitudinal vortices in the boundary layer along a concave wall," J. Geophys. Res. 67, 3075-3080 (1962).

13. Wortmann, F.X., "Experimental investigations of vortex occurrence at transition in unstable laminar boundary layers," p. 815, Munich: Proceed. XI Int. Congr. Appl. Mech. 1964.

14. Wortmann, F.X., "Visualization of transition," J. Fluid Mechanics 38, 3473-3480 (1969)

15. Tani, I., Aihara, Y., "Görtler vortices and boundary layer transition," Z. Angew. Math. Phys. 20/39, 309 (1969).

16. Clutter, D.W., Smith, A.M.O. and Brazier, J.G., "Techniques of flow visualization using water as the working medium," Douglas Aircraft Comp., Inc., Report No. ES 29075 (1959).

17. Hama, F.R., "Boundary layer transition induced by a vibrating ribbon on a flat plate," University of Maryland, Techn. Note BN 195, AFOSR-TN 60-290 (1960).

18. Geller, E.W., "An electrochemical method of visualizing the boundary layer," Master Thesis, Dept. of Aeron. Engr. Mississippi State College, 1954.

19. Lukasik, .SJ. and Grosch, C.E., "Velocity measurements in thin boundary layers," Davidson Laboratory, Stevens Institute of Technology, Hoboken, New Jersey, Technical Memorandum, 1959. /179

20. Schraub, F.A., Kline, S.J., Henry, J., Runstadler, P.W. and Litell, A., "Use of hydrogen bubbles for qualitative dertermination of time dependent velocity fields in low speed water flows," Report MD-10, Thermoscience Div. Mech. Engr. Dept. Stanford Univ., 1964.

21. Rinner, K., "The law of imagery and orientation problems in two-dimensional photogrammetry," Special Vol. No. 5 of the Austrian Journal for Measurement Techniques (1948).

22. Mori, Ch. and Okamoto, A., "Approximation methods for determining the position of an underwater point in two-dimensional photogrammetry," Mem. Fac. Engr., Kyoto Univ. 33/1 47-65 (1970).

23. Tewinkel, G.C., "Water depths from aerial photographs," Photo Engr., 1037 (1963)

24. Graefe, V., "Construction of a low-turbulent water tank for studying unstable boundary layers and measuring the degree of turbulence of the flow in the tank," Max Planck Institute for Flow Research, Göttingen, Report 5 (1968).

25. Schubauer, G.B., Skramstad, H.K., "Laminar boundary layer oscillations and stability of laminar flow," National Bureau of Standards, Research paper 1772, (1943).

26. Schubauer, G.B., Spangenberg, W.G. and Klebanoff, P.S., "Aerodynamic characteristics of damping screens," NACA TN 2001 (1950).

27. Bradshaw, P., "The effect of wind tunnel screens on nominally two-dimensional boundary layers," J. Fluid Mech. 22/4, 679-687 (1965)

28. Mochizuke, M., "Smoke observation on boundary layer transition caused by spherical roughness element," J. Phys. Soc. Japan 16/5 (1961).

29. Menzel, K. "On a nonlinear three-dimensional instability of laminar boundary layer flows," DLR FB 69-48 (1969).

30. Stuart, J.T. "The production of intense shear layers by vortex stretching and convection," Advisory Group for Aeronautical Research and Development, Report 514 (1965).

31. Meksyn, D. and Stuart, J.T., "Stability of viscous motion between parallel planes for finite disturbances," Proc. Roy. Soc. Ser. A 208, 517-526 (1951)

32. Grohne, D., "The stability of flat tunnel flow in comparison with three-dimensional disturbances of finite amplitude," AVA Report 69A30 (1969).

33. Murphy, J.S., "Extensions of the Falkner-Sean similar solutions to flows with surface curvature," AI[illegible] Journal 3, 11 (1965).

34. Narasimha, R. and Ojha, S.K., "Effect of longitudinal surface curvature on boundary layers," J. Fluid Mech. 29/1, 187-199 (1967).

35. Nutant, J.A., The Transition Process in a Boundary Layer on a Flat Plate, Maryland University, College Park, Ph.D. Thesis, Contr. AF 49, pp. 1-80.

36. Hama, F.H. and Nutant, J., Detailed Flow-Field Observations in the Transition Process in a Thick Boundary Layer, Proc. Heat Transfer and Fluid Mech. Inst. Vol. 77, Stanford University Press (1963).

37. Meyer, K.A. and Kline, S.J., "A visual study of the flow model in the later stages of laminar-turbulent transition on a flat plate," Report MD-7, Thermosciences Div., Mech. Engineering Dept., Stanford University (1961).

38. Kovasznay, L.S.G., Komoda, H and Vasudeva, B.R., Detailed Flow Field in Transition, Proc. 1962 Heat Transfer and Fluid Mech. Inst., Stanford University Press, (1962).

39. Klebanoff, P.S., Tidstrom, K.D. and Sargent, L.M., "The three-dimensional nature of boundary layer instability," J. Fluid Mech. 12/1, 1-33 (1962). /180

40. Komoda, H., "Nonlinear development of disturbance in a laminar boundary layer," Phys. Fluids 10, Suppl. 87 (1967).

41. Idrac, P., Experimental Studies on Sail Flight, Dissertation, Paris, 1921.

42. Görtler, H., "On an analoby between the instabilities of laminar boundary layer flows on concave walls and on heated walls," Ing.-Arch. 28, 71-78 (1959)

43. Kirchgässner, K., "A few examples for the stability theory of flows on concave and heated walls," Ing.-Arch. 31/2, 115-124 (1962).

44. Finsterwalder, R. and Hofmann, W., Photogrammetry, Walter de Gruyter & Co., Berlin, 1968.